MEASUREMENTS OF DAMPING FOR NONDESTRUCTIVELY ASSESSING THE INTEGRITY OF FIBER REINFORCED COMPOSITES

By

BAI-TANG LEE

A DISSERTATION PRESENTED TO THE GRADUATE SCHOOL OF THE UNIVERSITY OF FLORIDA IN PARTIAL FULFILLMENT OF THE REQUIREMENTS FOR THE DEGREE OF DOCTOR OF PHILOSOPHY

UNIVERSITY OF FLORIDA

1985

ACKNOWLEDGMENTS

The author wishes to express his appreciation for the assistance and support provided by all the members of his supervising committee. He is grateful to Dr. B.M. Leadon for permission to use his laboratory for the instrument and study, and to Dr. D.H. Liu for his timely suggestions and insight. The author also wishes to thank his wife, Yen-Jeng, for taking such nice care of the whole family.

January 2, 1985

TABLE OF CONTENTS

		Page
ACKNOWLEDGMENTS		ii
LIST OF TABLES		v
LIST OF FIGURES		vi
ABSTRACT		x
CHAPTER 1	INTRODUCTION	1
	1.1 Introduction	1
	1.2 Literature Survey	2
	1.3 Scope of the Present Investigation.	10
	1.4 Layout of the Dissertation	10
CHAPTER 2	DAMPING	13
	2.1 Introduction	13
	2.2 Mechanisms of Damping	15
	2.2.1 Viscous Damping	15
	2.2.2 Hysteretic Damping	16
	2.2.3 Coulomb Damping	19
	2.3 Types of Definitions of Damping Units	20
	2.3.1 Damping Properties of Materials	20
	2.3.2 Damping Properties of Dynamic Systems	21
	2.4 Methods of Damping Measurement	24
CHAPTER 3	COMPOSITE MATERIAL DAMPING USING IMPULSE TECHNIQUE	29
	3.1 Introduction	29
	3.2 Frequency Domain Measurements	30
	3.2.1 Frequency Response Function	31
	3.2.2 Coherence Function	33
	3.3 Experimental Procedures and Improvements	35
	3.4 Experimental Results and Discussion	51

CHAPTER 4 EVALUATION OF DAMAGE BY DAMPING MEASUREMENTS 59

4.1 Introduction 59
4.2 Sensitivities of Damping and Resonant Frequency to Local Damage 61
4.3 Behavior of Damping Due to Local Damage 63
4.3.1 Correlation Between Damage and Damping 68
4.3.2 Sensitivity of Damping to Local Damage 75
4.4 Studies on Damping Due to Damage From Artificial Delaminations and Three-Point Bending Tests 81

CHAPTER 5 METHOD OF LOCATION AND SEVERITY OF DAMAGE 94

5.1 Introduction 94
5.2 Description of the Method 94
5.3 Evaluation of the Method 100

CHAPTER 6 SUMMARY AND CONCLUSIONS 113

6.1 Summary of the Results 113
6.2 Conclusions 117

APPENDIX A DERIVATION OF EQS. (2.15) FOR THE CASES OF VISCOUS DAMPING AND COMPLEX STIFFNESS REPRESENTATION OF DAMPING ... 119

APPENDIX B TABULATED DATA--MEASURED DAMPING VALUES FOR SMC R50 SPECIMENS 128

APPENDIX C TABULATED DATA--MEASURED DAMPING VALUES FOR KEVLAR/EPOXY SPECIMENS 136

APPENDIX D TABULATED DATA--MEASURED DAMPING VALUES FOR HYBRID COMPOSITE G4 SPECIMENS 143

REFERENCES 150

BIOGRAPHICAL SKETCH 156

LIST OF TABLES

Table		Page
3.1	Specimen dimensions	37
3.2	Comparison of experimental results with contact and non-contact probes	52
3.3	Comparison of experimental results using base-band measurement and zoom measurement	54
3.4	Final experimental results	55
4.1	Mode numbers of damping which are the most sensitive to damage at various positions of the damage	80
4.2	Results of damping measurements of $[90_5/0_4/90_5]$ glass/epoxy specimens with inserts to represent artificial delaminations	88
4.3	Results of damping measurements of 16-ply unidirectional glass/epoxy specimens with unglued area to represent artificial delaminations	89
4.4	Results of damping measurements of $[90_2/0_{10}/90_2]$ glass/epoxy specimens with damage due to three-point bending tests	90
5.1	Actual and evaluated positions and severities of damage of SMC R50 specimens	107
5.2	Actual and evaluated positions and severities of damage of Kevlar/epoxy specimens	108
5.3	Actual and evaluated positions and severities of damage of hybrid composite G4 specimens	109
5.4	Damage resulted in 3-point bending tests evaluated by equivalent percent reduction of total thickness	111

LIST OF FIGURES

Figure		Page
2.1	Force-displacement curve of viscous damper	16
2.2	Hysteresis loop of material under simple harmonic motion	18
2.3	Definition of f_a and f_b used for damping calculation	23
3.1	Ideal single input/single output system	31
3.2	Single input/single output system with extraneous noise	31
3.3	Original schematic drawing of the impulse technique	36
3.4	Typical imaginary and real parts of frequency response function	39
3.5	Schematic drawing of the modified impulse hammer experimental set-up	41
3.6	A photographic view of the experimental set-up.	43
3.7	Comparison of coherence with contact and non-contact probes	44
3.8	Comparison of coherence with and without amplifier	45
3.9	Comparison of transfer function with and without amplifier	46
3.10	Photographic view of spring attached to the hammer	48
3.11	Imaginary part of the transfer function with and without spring control	49
3.12	Coherence function with and without spring control	50

4.1 The damaged beam 62

4.2 Percent damping and frequency differences between damaged and undamaged conditions vs. severity of the damage--1st mode 64

4.3 Percent damping and frequency differences between damaged and undamaged conditions vs. severity of the damage--2nd mode 65

4.4 Percent damping and frequency differences between damaged and undamaged conditions vs. severity of the damage--3rd mode 66

4.5 Specimen loss factor vs. severity of damage at x/ℓ = 0.033, 0.15, and 0.48--1st mode 69

4.6 Specimen loss factor vs. severity of damage at x/ℓ = 0.3, 0.7, 0.82, and 0.91--1st mode 70

4.7 Specimen loss factor vs. severity of damage at x/ℓ = 0.033, 0.15, and 0.48--2nd mode 71

4.8 Specimen loss factor vs. severity of damage at x/ℓ = 0.3, 0.7, 0.82, and 0.91--2nd mode 72

4.9 Specimen loss factor vs. severity of damage at x/ℓ - 0.033, 0.15, and 0.48--3rd mode 73

4.10 Specimen loss factor vs. severity of damage at x/ℓ = 0.3, 0.7, 0.82, and 0.91--3rd mode 74

4.11 Percent damping difference between damaged and undamaged conditions vs. severity of the damage--SMC R50 specimen 77

4.12 Percent damping difference between damaged and undamaged conditions vs. severity of the damage--Kevlar-epoxy specimen 78

4.13 Percent damping difference between damaged and undamaged conditions vs. severity of the damage--hybrid composite G4 specimen 79

4.14 Percent damping difference between damaged and undamaged conditions vs. severity of the damage for SMC R50 and Kevlar-epoxy specimens at x/ℓ = 0.033 82

4.15 Percent damping difference between damaged and undamaged conditions vs. severity of the damage for SMC R50 and hybrid composite G4 specimens at $x/\ell = 0.033$ 83

4.16 Layout for artificial delamination inserts in two interfaces of $[90_5/0_4/90_5]$ glass/epoxy beam specimens 85

4.17 Artificial delaminations represented by the unglued portion in the middle plane of 16-ply unidirectional glass/epoxy specimens 86

5.1 Percent damping difference between damaged and undamaged conditions vs. locations of damage for various severities of the damage--1st mode (SMC R50 specimen) 95

5.2 Percent damping difference between damaged and undamaged conditions vs. locations of damage for various severities of the damage--2nd mode (SMC R50 specimen) 96

5.3 Percent damping difference between damaged and undamaged conditions vs. locations of damage for various severities of the damage--3rd mode (SMC R50 specimen) 97

5.4 Percent damping difference between damaged and undamaged conditions vs. locations of damage for various severities of the damage--1st mode (Kevlar-epoxy specimen) 101

5.5 Percent damping difference between damaged and undamaged conditions vs. locations of damage for various severities of the damage--2nd mode (Kevlar-epoxy specimen) 102

5.6 Percent damping difference between damaged and undamaged conditions vs. locations of damage for various severities of the damage--3rd mode (Kevlar-epoxy specimen) 103

5.7 Percent damping difference between damaged and undamaged conditions vs. locations of damage for various severities of the damage--1st mode (hybrid composite G4 specimen) 104

5.8 Percent damping difference between damaged and undamaged conditions vs. locations of damage for various severities of the damage--2nd mode (hybrid composite G4 specimen) 105

5.9 Percent damping difference between damaged and undamaged conditions vs. locations of damage for various severities of the damage--3rd mode (hybrid composite G4 specimen) 106

Abstract of Dissertation Presented to the Graduate School of the University of Florida in Partial Fulfillment of the Requirements for the Degree of Doctor of Philosophy

MEASUREMENTS OF DAMPING FOR NONDESTRUCTIVELY ASSESSING THE INTEGRITY OF FIBER REINFORCED COMPOSITES

By

Bai-Tang Lee

May 1985

Chairman: Chang-Tsan Sun
Major Department: Engineering Sciences

The development of an experimental method to measure material damping and the assessment of the utility of damping measurements as a tool for quantitatively assessing the integrity of fiber reinforced composites were undertaken. An impulse technique using a non-contact probe displacement motion transducer was developed for the measurement of material damping up to the third mode of vibration.

The test specimens, fixed-free beams vibrating transversely, were fabricated from five types of composite materials. They were graphite/epoxy, Kevlar/epoxy, and glass/epoxy continuous fiber composites, chopped glass fiber composite, and hybrid composite.

The severity of damage simulated by milling-machine cuts correlates well with increased damping. There were no

significant changes in damping of the specimens having mylar inserts to represent delaminations. This is attributed to three factors: (1) the inserts being bonded with the material, (2) material damping variation between the specimens being more than the damping change due to inserts, (3) the variation in damping due to clamping at the mounting base being more than the damping change caused by the mylar inserts. The first factor can be improved by the delaminations represented by an unglued portion; for this type of damage, the severity of the damage correlating well with increased damping has been observed. For the type of damage from bending tests, no significant changes in damping were observed. This may be attributed to the fact that the damping changes due to damage of the matrix-crack type are masked in small-amplitude vibration by the variation between the specimens.

An example is given to describe a graphic method to approximately locate and quantify damage. The results of the method give correct ranges in evaluations of the location and severity of the damage by milling-machine cuts.

The use of the damping measurements for nondestructively assessing the integrity of fiber reinforced composite materials has been quite successful for the case of milling-machine cuts. However, this technique has certain limitations. An ability to make measurements of damping in higher modes of vibration may be necessary to be able to detect microdamage.

CHAPTER 1
INTRODUCTION

1.1. Introduction

The need to develop and use light-weight structural components in the design of aircraft and automotive vehicles has brought increasing applications of composite materials. Composites have various kinds of flaws [1] built into them during the manufacturing process. Similar looking composites (on visual appearance) may have quite different properties depending upon their internal features. Reliable performance of the advanced, high-strength materials in critical applications depends on assuring that each part placed in service satisfies the conditions assumed in design. It is therefore needed to insure the quality of materials used and the integrity of the product during various stages of manufacture and also the final product. This development has produced the need to handle nondestructive testing and quality control more systematically. Nondestructive tests are different from all tests and measurements which damage the serviceability of the items tested. Destructive tests can be made only on a few prototypes or on a small percentage of production parts. With increasing complexity of structures and severity of service loads, percentage testing to

destruction can be inadequate to insure the reliability of the critical components of modern engineering systems.

Many methods of nondestructive testing have been developed. However, all of these tests have disadvantages as well as advantages, and there is no method which is universally applicable [2]. Some methods, such as ultrasonic C-scan, require access to the whole of the structure and involve time-consuming, scanning of the whole surface. Thus, measurement of dynamic characteristics, that is, the resonant frequencies and damping, of a structure is potentially a very attractive form of nondestructive test since these properties can be measured at a single point on the structure and are independent of the position chosen. Specifically, damping has the advantage of being far more sensitive to damage than resonant frequency is. Therefore, the choice was made to develop a reliable method and to assess the utility of damping measurements as a tool for quantitatively assessing the integrity of fiber reinforced composites.

1.2. Literature Survey

There is a need to develop nondestructive testing techniques for composite materials suitable for the determination of component quality after fabrication and for the assessment of degradation throughout service. Methods of nondestructive testing suitable for composite materials will be described in this section.

Damage growth is generally accompanied by stiffness change. Hence, damage growth can be monitored indirectly through stiffness [3-5]. In these works of fatigue tests on composite materials, correlations between damage growth and stiffness changes were noted and rapid stiffness loss occurring early in the fatigue life time was observed. All of these efforts have demonstrated the possibility of using stiffness measurement as a tool of nondestructive testing.

When a material is subjected to loads, it emits low level sound, a phenomenon known as acoustic emission [6]. This characteristic enables the technique of acoustic emission to be successfully used to detect and quantify flaws in a material nondestructively [6-10]. Dunegan et al. [6], in their work on fracture analysis, showed that there is a marked difference between the acoustic emission from an unflawed tensile specimen and one containing a sharp crack. The technique of acoustic emission is based on the detection of the stress pulse generated by the strain energy released during deformation and fracture of the material. The stress waves are normally detected by a piezo-electric transducer, and the resultant electrical signal can be processed in one of several ways (e.g., event counting, ring-down counting, count rate or total count) [7, 11]. The damage will only be detected if it occurs during monitoring by the acoustic emission technique. The necessity to apply an appreciable stress to the specimen contrasts with most testing techniques.

It is known that ultrasonic waves undergo energy dissipation while propagating through materials because of viscous friction, elastic hysteresis, and interaction of the waves with inhomogeneities [12]. Ultrasonic attenuation can be a useful parameter for characterizing the defects of materials [13-17]. Williams and Lampert [13] investigated the ultrasonic characterizations of graphite-fiber composites subjected to drop-weight impact testing. The results were correlated with the number of impacts and the composite residual tensile strength. These correlations strongly suggest that impact damage in graphite fiber composites can be nondestructively assessed quantitatively by using the through-thickness attenuation. Joshi and Green [14] used ultrasonic attenuation measurements to detect the fatigue damage. They showed that the attenuation increases with the severity of the damage. Ultrasonic inspection is usually performed by one of two basic methods, namely pulse-echo and through transmission. Basically a high-frequency sound (1 to 25 MHz) is emitted in periodic bursts from an ultrasonic transducer through a coupling medium into the specimen being inspected. The resulting attenuated pulse emerging from the specimen is picked up by the transmitting transducer (pulse-echo method) or by a separate receiving transducer (through transmission method). The information from it is electronically processed and the data are displayed from the evaluation of presence, size, and location of flaws.

In ultrasonic inspection, material inhomogeneity and anisotropy severely limit the capability for characterizing discrete flaws. As a result, necessary size, shape, and position information on flaws is obtained with much less accuracy than in homogeneous materials [18].

The techniques of radiography have played an important role in the determination of the quality of materials. A radiograph is a photographic record produced by the passage of X-ray or gamma rays through a test specimen onto a film. The radiograph indicates density differences in the specimen. Therefore, it can be used to indicate flaws as long as the resulting density differences produce a radiation attenuation sufficient to cause a contrast on the film [1, 19-21]. Tober and Schnell [1] established an X-radiography technique which permits the safe detection of single 0.4 mm diameter voids at a carbon-fibre-reinforced-plastics (CFRP) laminate thickness of 2 mm or 0.8 mm diameter voids at 8 mm thickness. The technique is also an excellent means of detecting inclusions, fiber direction, resin-rich or resin-starved areas. Chang et al. [19] used X-ray nondestructive testing to observe the fatigue damage initiation and growth within graphite/epoxy composite. In X-ray radiography, electromagnetic energy is supplied from a source. Penetrating radiation proceeds in straight lines to the object being tested. Some of the rays pass through the material and others are absorbed. The fraction transmitted depends upon the nature of the material and its thickness. If the specimen is

uniform in density and thickness, the radiation emerging from the opposite side of the specimen will be of uniform intensity. If a specimen has variations in thickness or density due to inhomogeneities, the intensity of the emerging radiation will be modified. This emerging radiation is projected onto a film. The darker regions on the developed film represent the more penetrable parts of the specimen and the lighter regions the more opaque. Thus, the radiography technique can be used to detect flaws within materials.

The actual inspection techniques in use are quite varied and each has limited application. The capabilities and limitations of various techniques are briefly reviewed by Stone [22]. This means that several different inspection techniques must be used to determine the integrity of any component [1, 16].

In a vibration technique, the test body itself is caused to vibrate freely. Many physical characteristics of the body may be determined from the characteristics of the induced vibration. Changes in stiffness, whether local or distributed, lead to changes in natural frequencies of a vibrating system. Adams et al. [2] successfully tested the frequency measurement on structures which could be treated as one-dimensional and vibrating longitudinally. Closed-form analytical techniques using receptance theory [23] were presented for the one-dimensional structures. Damage of the structures was represented by a spring having a stiffness K_x. If K_x is infinite, there is no damage, while decreasing

values of K_x indicate increasing damage. It was found that the minimum amount of damage to be detected is equivalent to the removal of 1% of the cross-sectional area of the structure at a single location. Excellent agreement was also obtained between the evaluated and actual damage sites. The method of vibration technique with frequency measurement developed for one-dimensional structures can be used to detect and locate damage without the need for access to the whole structure. The method requires access to only one point of the structure. Springer [24] used a reduced cross-sectional area to represent damage within structures and extended the method to include both the longitudinal and transverse vibration of uniform bars containing a symmetric discontinuity in cross-sectional area. The method for longitudinal vibration to detect, locate, and quantify the damage simulated by saw cuts was a great success. In the transverse vibration case, the presence of damage did result in a measurable shift in the natural frequencies. However, the method did not give satisfactory results in evaluation of the location and magnitude of the damage.

Cawley and Adams [25] extended the natural frequency method to two-dimensional structures. The analysis of one-dimensional structures was carried out using receptance theory. There is no two-dimensional equivalent of the receptance theory, so finite element analysis was chosen by Cawley and Adams [25]. The tests on two-dimensional structures were carried out using flexural vibration. Damage introduced to

the plate included hole, saw cut, and crushing in a hydraulic press. The results from aluminum and cross-ply CFRP plates show that the proposed finite element scheme can be used to detect, locate and roughly quantify damage in structures. In the later application of the scheme, they reported a series of tests performed in order to test the applicability of the method to structures fabricated from fiber reinforced plastics [26]. Several types of damage were again employed including holes, saw cuts, local heating, impact and crushing in a hydraulic press. The results indicate that damage equivalent to the removal of about 0.1% of the area of a shell structure can be detected. The applicability of the method to evaluate the damage was confirmed.

Vibration techniques can be also used to measure material damping. Relatively little attention has been paid to the use of damping measurement for the determination of structural integrity. Lifshitz and Rotem [27] used a vibration technique to measure the complex dynamic moduli and damping of tensile specimens. The specimens used were epoxy and polyester composites filled with sand particles. Damage was represented by stress induced structural changes in composites. The experimental results indicate that the dynamic moduli decreased about 10% and the damping increased about 40% when the specimens were loaded to failure. Schrager [28] used a torsion pendulum as a nondestructuve monitor of two types of epoxy resin specimens. Complex dynamic modulus and material damping were measured during fatigue tests.

Specimens with a large degree of crosslinking exhibited a regular decrease of storage modulus (i.e., of the in-phase component of the dynamic modulus) and an increase of damping with the number of fatigue cycles. These changes were recovered after 20 hours when the fatigue test was interrupted at 34,000 cycles. Specimens with less crosslinking exhibited a small initial increase in modulus followed by a decrease. The damping uniformly increased a small amount. Both the decay of modulus and the increase in damping reflect changes in the fatigue state of a specimen.

The sensitivities of damping and stiffness to the presence of damage have been compared by some researchers. Adams et al. [29] used measurements of the shear modulus and of the damping coefficient in torsion to detect damage in CFRP rods, and it was found that the damping was a much more sensitive indicator. Gibson and Plunkett [30] tested unidirectional and crossplied E-glass/epoxy specimens in flexural vibration. Increased damping and decreased stiffness were observed when the specimens were damaged in large amplitude tests. The resulting increase in damping is much more significant than the corresponding reduction in stiffness.

The correlation of the severity of damage with increased damping has also been investigated by several investigators [31-33]. In all of these efforts, measurements of damping and stiffness have been used to detect damage. The severity of damage correlates well with increased damping. However,

attempts have not been made to evaluate the position and magnitude of the damage. With the impulse technique used in this study, damping of higher modes of vibration can be measured simultaneously. This offers a possibility to locate and quantify the damage.

1.3. Scope of the Present Investigation

The main purpose of this work is to assess the ability of damping measurements to detect, locate, and quantify damage. The work presented in this dissertation is limited to four objectives as follows:

A. To develop the impulse technique to measure material damping.

B. To measure material damping from beams vibrating transversely with milling-machine cuts to represent damage and to assess the ability of damping measurements to detect damage.

C. To extend the procedures and techniques established in A and B above to the cases of damage from artificial delaminations and three-point bending tests.

D. To introduce a graphic method to locate and quantify damage from measured damping values.

1.4. Layout of the Dissertation

The organization of the dissertation includes six chapters.

In Chapter 1, the necessity to develop nondestructive testing technique is highlighted. A survey of the state of the art of nondestructive inspection is presented. The precise subject to be considered and the reasons for considering the subject are described in detail.

Chapter 2 is devoted to more information on damping. The mechanisms of damping and types of definition of damping units are included. Methods of damping measurement are surveyed in the last section of the chapter.

Chapter 3 establishes an experimental method of impulse technique using a non-contact probe displacement motion transducer to pick up the response signal for the determination of material damping. The digital fast Fourier analyzer in the impulse technique performs a variety of time-domain and frequency-domain measurements. The principle of the impulse technique in the frequency-domain measurements is considered in the first portion of the chapter. Two functions are introduced, namely the frequency-response function and the coherence function. In the second portion of the chapter, an experimental method of the impulse technique with some improvements to measure material damping is developed. The experimental results and discussion are presented in the third portion of the chapter.

In Chapter 4, the ability of damping measurements to determine the damage state are assessed. In the first portion of the chapter, sensitivities of damping and resonant frequency to local damage are compared. Behaviors of

damping due to local damage are described in the second portion of the chapter. Damage is simulated by milling-machine cuts in this portion of the work. Correlation between damage and damping is investigated. The sensitivity of damping to local damage is also examined in this portion to give a complete understanding of the behavior of damping due to local damage. In the third portion, studies on damping due to damage from artificial delaminations and from three-point bending tests are reported. The ability to detect damage from damping measurements in these more realistic cases is investigated.

Chapter 5 describes a graphic method to roughly locate and quantify damage from the measured damping values. An example is given to illustrate the method in the first portion of the chapter. In the second portion, the method is evaluated to confirm further its correctness.

In Chapter 6, a summary is presented of the results obtained during this study and the conclusions derived from those results are given.

CHAPTER 2
DAMPING

2.1. Introduction

The phenomenon in which the amplitude of vibration steadily diminishes is called damping. In damping, the energy of the vibrating system is dissipated through friction as heat [34]. Damping is responsible for the eventual decay of free vibrations and provides an explanation for the fact that the response of a vibratory system excited at resonance does not grow without limit [35]. The mechanisms of damping can take any of several forms, and often more than one form may be present at a time.

In viscous damping, the damping force is proportional to velocity. In dry friction or coulomb damping, the damping force is a constant. It is caused by kinetic friction between sliding dry surfaces. Solid damping or hysteresis damping [23] is caused by the internal friction or hysteresis when a solid is deformed.

Various forms of description of damping have appeared in the literature. Several types of definition of damping units in terms of properties of materials and dynamic systems are described in this chapter.

Measuring material damping has become of interest in engineering applications. Most damping measurements rely either on decay, resonant dwell, or band-width. The decay test measures free vibration decay of a specimen after its release from an initial displacement [36]. The resonant-dwell test and the band-width test are forced-vibration techniques. The resonant-dwell test involves use of a dynamic shaker to excite the specimen and measurements of the resonant mode shape of the specimen [37]. In the band-width test, the shape of the amplitude versus frequency function is determined; the resonant peak and the amplitudes at frequencies below and above resonance, usually at the two half-power points [38], are measured.

The relatively new impulse hammer technique [39], which is in the class of transient excitation, was used in this research. The advantages of this technique are

(a) An impulse force will excite all resonances within its useful frequency range.

(b) Portability is made possible.

(c) No elaborate specimen fixture is necessary.

(d) No electromechanical exciters are required.

(e) Testing time is greatly reduced.

2.2. Mechanisms of Damping

2.2.1. Viscous Damping

This model has a clear physical meaning. Energy is dissipated by fluid friction. A typical application is the dash pot. The damping force, F_D, is proportional to the velocity of the motion, $\dot{x}$:

$$F_D = -c\dot{x} \tag{2.1}$$

where c is the viscous damping constant. The negative sign indicates that the damping force is opposite to the direction of the velocity.

The dissipated energy during one cycle of a harmonic motion, $x = X \sin \omega t$, will be

$$D = \int_0^{\frac{2\pi}{\omega}} c\left(\frac{dx}{dt}\right)^2 dt = \int_0^{2\pi} cX^2\omega\cos^2\omega t \, d(\omega t) \tag{2.2}$$

$$= \pi c X^2 \omega$$

Here ω is the circular frequency in radians per unit time, equal to 2π times the frequency in cycles per unit time.

Alternatively, if an external force, f_e, was supplied just sufficient to balance the damping force and to maintain a simple harmonic motion, $x = X \sin\omega t$, then

$$f_e = c\frac{dx}{dt} = cX\omega\cos\omega t \tag{2.3}$$

If this force as a function of displacement is plotted, an ellipse is obtained as shown in Fig. 2.1.

$$\left(\frac{x}{X}\right)^2 + \left(\frac{f_e}{cX\omega}\right)^2 = 1 \qquad (2.4)$$

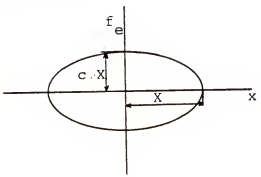

Fig. 2.1. Force-displacement curve of viscous damper

The area of the ellipse is the energy dissipated per cycle, $D = \pi c X^2 \omega$. The energy dissipated is proportional to the frequency and to the square of the amplitude of motion.

2.2.2. Hysteretic Damping

Using viscous damping to represent the internal damping of materials or the damping of a built-up structure may incur a serious error. The energy dissipated per cycle in viscous damping increases with frequency [34]. For many engineering materials, it has been observed that the energy dissipated per cycle in internal damping is independent of frequency, at least in a certain frequency range [40, 41]. Other cases have, however, shown frequency dependence [37, 38].

The hysteretic damping model has been designed to cover the frequency-independent case. The simplest device that can be used to represent this kind of internal damping is to assume that the damping force is proportional to velocity and inversely proportional to frequency. This type of damping is called hysteretic damping, since it can be directly related to the hyspteresis loop [42].

If the behavior of material is modeled by an elastic spring in parallel with a hysteretic damping element, the total force F_T is the sum of the spring force and the damping force,

$$F_T = -kx - \frac{h}{\omega}\dot{x} \tag{2.5}$$

where h is the hysteretic damping constant.

If an external force f_e is applied just sufficient to balance the damping force and to maintain a simple harmonic motion, $x = X\sin\omega t$, then

$$f_e = kx + \frac{h}{\omega}\dot{x} \tag{2.6}$$

Plotting force as a function of displacement in the x-direction yields the skewed ellipse of Fig. 2.2.

$$(\frac{x}{X})^2 + (\frac{f_e - kx}{hX})^2 = 1 \tag{2.7}$$

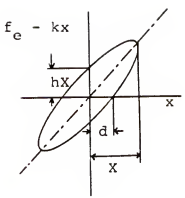

Fig. 2.2. Hysteresis loop of material under simple harmonic motion.

The energy dissipated for one cycle of motion is

$$D = \int_0^{\frac{2\pi}{\omega}} F_T \left(\frac{dx}{dt}\right) dt$$

$$= \int_0^{2\pi} kX^2 \omega \sin\omega t \cos\omega t \; d(\omega t) + \int_0^{2\pi} hX^2 \cos^2\omega t \; d(\omega t)$$

$$= \pi h X^2 \qquad (2.8)$$

Thus, the energy dissipated per cycle is dependent only on the constant h and the amplitude of motion.

The hysteretic damping constant is a measure of the hysteresis loop of Fig. 2.2 and is a property of the material or structure. The intercept of the hysteresis loop on the force axis depends on the value of the hysteretic damping constant h and the maximum displacement X. If d is the intercept of the hysteresis loop on the displacement

axis, the following approximate equation holds for light damping

$$\frac{h}{k} \cong \frac{d}{X} \tag{2.9}$$

In the case of light damping, the value of d is small in comparison to X, and it is sufficient to evaluate the hysteretic damping constant by the approximate ratio of Eq. (2.9).

Lazan [43] notes that in general a phenomenological relation for the energy dissipated in each cycle is

$$D = J\sigma_a^n \tag{2.10}$$

where J and n are material constants,

σ_a = Stress amplitude.

The term, linear damping, should satisfy two conditions:

(a) damping exponent, n = 2, and

(b) the hysteretic loop is elliptical in form.

2.2.3. Coulomb Damping

Coulomb damping results from the sliding of two dry surfaces. The damping force is equal to the product of the normal force N and the coefficient of friction μ and is assumed to be independent of the velocity, once the motion is initiated.

The decay in amplitude per cycle of free vibration is a constant and equal to

$$X_n - X_{n+1} = \frac{4\psi N}{k} \tag{2.11}$$

where X_n is the amplitude of n^{th} cycle and k is the constant of the spring in parallel with the damping element.

Two interesting facets of coulomb damping or dry friction are significant:

(1) The natural frequency is unaltered by dry friction damping, i.e., $\omega_d = \omega_n$.

(2) The amplitudes of free vibration decay linearly with time.

This contrasts with viscous damping where the damped free vibration circular frequency is

$$\omega_d = \omega_n\sqrt{1 - \xi^2}, \quad \xi = \text{damping ratio},$$

as shown in Appendix A, and the amplitudes decay exponentially with time.

2.3. Types of Definitions of Damping Units

Various definitions of damping are listed in this section in terms of damping properties of materials and dynamic systems.

2.3.1. Damping Properties of Materials

A. Specific damping capacity, ψ

The specific damping capacity is defined as the energy loss per cycle D divided by the peak potential energy,

$$\psi = \frac{D}{U}$$

B. Loss coefficient or Loss factor, η

The Loss factor is defined as the ratio of energy loss per radian $D/2\pi$ divided by the peak potential or strain energy U,

$$\eta = \frac{D}{2\pi U} \tag{2.12}$$

C. Complex Modulus, E^*

For linear viscoelastic materials, the complex modulus notation can be applied.

$$E^* = E' + iE'' = E'(1 + i\eta) \tag{2.13}$$

where E' = storage Young's modulus

E'' = Loss Young's modulus

$\eta = \frac{E''}{E'}$ = Loss factor

2.3.2. Damping Properties of Dynamic Systems

A. Logarithmic decrement

In a linear system, free vibrations decay exponentially. The larger the damping, the faster is the decay. Thus, the logarithmic decrement is defined as follows:

$$\delta = \ln \frac{X_a(n)}{X_a(n+1)} \tag{2.14}$$

where $X_a(n)$ is the amplitude of n^{th} cycle.

For a single-degree-of-freedom spring-mass-damper system, the following approximate relations hold.

$\delta = \pi\eta$ and also

$$\delta = 2\pi\xi \tag{2.15}$$

where η = loss factor,

and ξ = damping ratio, $\frac{c}{c_c}$.

In the definition of the damping ratio, c_c is the critical damping of the viscous damper. The derivation of Eqs. (2.15) is given in Appendix A for the cases of viscous damping and complex stiffness representation of damping.

B. Band width of half-power points

The separation $(\omega_2 - \omega_1)$ between the frequencies associated with the half-power points increases with an increase in damping and thus can be used as a measure of damping. A more meaningful definition is to normalize by the associated damped resonant frequency (ω_r), i.e., to use the dimensionless band width given by

$$\frac{\omega_2 - \omega_1}{\omega_r}$$

and this is related to the damping property of materials by

$$\frac{\omega_2 - \omega_1}{\omega_r} = \eta$$

C. Quality factor, Q

The damping properties of a resonance can be described by a quality factor, Q [44], [45, 46].

$$Q = \frac{\omega_r}{\omega_2 - \omega_1} \tag{2.16}$$

$$= \frac{(\frac{f_a}{f_b}) + 1}{(\frac{f_a}{f_b}) - 1} \tag{2.17}$$

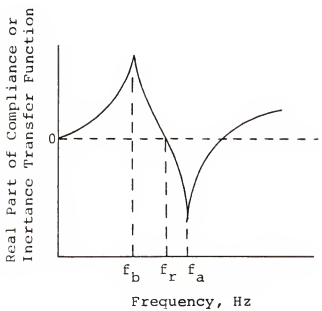

Fig. 2.3. Definition of f_a and f_b used for damping calculation.

where Compliance transfer function = displacement/force

Inertance transfer function = acceleration/force

f_a = frequency above resonance, where the real part of compliance or inertance reaches a peak,

and f_b = frequency below resonance, where the real part of compliance or inertance reaches a peak of opposite sign.

For small damping, the following relations hold [47].

$$Q = \frac{1}{2\xi} = \frac{1}{\eta} \tag{2.18}$$

Thus a high-Q system is one with low damping, and vice versa.

2.4. Methods of Damping Measurements

Several experimental techniques have been used to measure the internal damping of materials [48]. Free vibration decay, resonant-dwell, and band-width methods appear to be the most popular. The impulse technique, a relatively new concept, has received considerable attention of researchers. This technique has the advantage of being easy to apply, of generating higher modes of vibration, and of reducing testing time.

Schultz and Tsai [38] used decay and band-width methods to test aluminum and glass-fiber-reinforced composites in flexural vibration. The damping in unidirectional beams increased with increasing frequency, and there was strong dependence of damping on excitation amplitude in the first mode. The dependence of amplitude could have resulted from air damping since the tests were conducted in air. Kume, Hashimoto and Maeda [49] reported an analytical method to

estimate material damping in a cantilever beam. The analytical results have been confirmed experimentally by the band-width method for a solid steel cantilever beam. They showed that the experimental results have the same order of magnitude as the theoretical results when the maximum stress amplitude is less than 7×10^6 to 10^7 Pa (1,000 to 1,500 psi).

Granick and Stern [37] used the resonant-dwell method to examine the relations between material damping, stress amplitude, and frequency for Aluminum 2024-T4. Results showed that damping as measured in air was largely aerodynamic drag and was displacement-amplitude and frequency dependent. On the other hand, damping as measured in vacuum was wholly material damping, independent of stress amplitude up to 140 MPa (20,000 psi), and dependent on frequency.

In the resonant-dwell method, each damping measurement is made at a single frequency and amplitude. Gibson and Plunkett [50] determined the internal damping of beam specimens in resonant flexural vibration from measurements of input acceleration and resulting specimen-bending strain. A polyester clamping shoulder was molded to the middle of the double-cantilever specimen. The input acceleration (excitation) and resulting bending strain (response) were measured by using a piezoelectric accelerometer and electrical resistance strain gages, respectively. The use of strain gages is undesirable because of the cost of strain gages and

the specimen preparation time for the large number of specimens to be tested. Gibson, Yau and Riegner [51] in their improved forced-vibration technique used non-contacting proximity transducers (Kaman KD-2310-3 U eddy-current displacement measuring system) and removable aluminum clamping blocks instead of strain gages and polyester clamping shoulder to detect specimen response, and material damping was found from the resonant amplitude ratio. They concluded that the presence of the strain gages or the proximity transducers does not affect the measured properties significantly. In the comparison of the effects of the clamping method, they showed that the loss factor is 30% to 43% higher with polyester shoulder clamping than for aluminum block clamping. Thus, the modified technique gives more reliable damping data (loss factor) than the original technique.

The impulse technique offered greatly reduced test time and effort and a broader flexibility available with handling digital data [52, 53]. Impulsive testing is normally conducted using some form of an instrumented hammer. A force transducer is mounted to the head of the hammer, measuring the force input to the structure. An accelerometer is used to measure the response of the structure. The data are analyzed with a dual-channel Fourier analyzer. Each time the structure is struck with the hammer, both the impulse force and the response acceleration are captured by the Fourier analyzer, with the impulse force used as a transient capture trigger. These two transient time histories are

Fourier-transformed to yield the input and output spectra. Usually, the results of several transient excitations are averaged. In this situation, the most desirable procedure is to compute the cross spectrum between the input and response and the power spectrum of the input. The resultant averaged transfer characteristic is derived by dividing the cross spectrum by the input power spectrum. The results are displayed graphically. Damping and natural frequencies can be extracted from the displayed transfer characteristic.

Drake and Henderson [54] used the inpulse technique to investigate the response properties of aircraft components and candidate damping materials under room temperature, fuel exposure, and water environment. The results were compared with the more conventional analog sine sweep technique. It turns out that measured resonant frequencies and modal damping are essentially the same for the two methods.

Gordon and Wolfe [55] used the digital impact test technique to measure the dynamic properties of light-weight aircraft structures. Two different types of structures were tested: honeycomb and skin-stiffened panels. The results were compared with the analog sine sweep technique. The comparison indicated close agreement in the results. The use of the digital technique has resulted in a considerable savings in the man hours required to obtain the dynamic properties of the structures.

Henderson and Drake [56] described the use of Fast Fourier Transform (FFT) analysis with the impact technique

in the design of damping applications for eliminating resonant high-cycle fatigue in specific light-weight structural components. With FFT analysis, which enables rapid identification of resonant frequencies, mode shapes, and modal parameters, a designer can optimize viscoelastic damping material applications for real structures.

To pick up the response of the structure, in general, the accelerometer is attached. If the weight of the test specimen is small, this mass loading can be significant. One generally switches to a non-contacting displacement transducer when a light-weight specimen is tested. The development of the impulse technique using a non-contacting displacement probe to measure composite material damping will be discussed in the next chapter.

CHAPTER 3
COMPOSITE MATERIAL DAMPING USING IMPULSE TECHNIQUE

3.1. Introduction

The impulse technique has a distinct advantage of being able to generate all higher modes simultaneously. The development of the digital fast Fourier analyzer has opened this new technique to the test engineer involved in experimental vibration measurements. The Fourier analyzer performs a variety of time domain and frequency domain measurements. The transformation related to these domains is the Fourier transform. All measurements are performed using digital signal processing techniques. This approach involves filtering and sampling the input waveforms. The sampling process converts a voltage (at a certain point in time) into a numerical representation. These numbers are then processed digitally to produce the various calculations performed by the analyzer. The primary data output from a Fourier analyzer is the frequency response function which is a measure of a system's characteristics. The analyzer also calculates the coherence function which gives an indication of the quality of the data.

The impulse technique consists of the application of a force pulse at a point on the test structure and the

measurement of the response at another point. The input force and response signal are digitally processed by the analyzer to form the frequency response function or transfer function. Damping and natural frequencies can then be extracted from the output of the analyzer.

In this chapter, an experimental method of the impulse technique using a non-contact probe displacement motion transducer to pick up the response signal was developed. Material damping of 2024-T3 aluminum, E-glass/polyester, graphite/epoxy, Kevlar/epoxy, and Owens-Corning G4 hybrid composites was measured. The results were compared with that obtained by using a contact probe (accelerometer).

3.2. Frequency Domain Measurements

There are two important relationships in a single input/single output system to be considered, namely, the frequency response function and the coherence function. For an ideal single input/single output system, as shown in Fig. 3.1, the following relations hold [57].

$$G_{yy}(f) = |H(f)|^2 G_{xx}(f) \tag{3.1}$$

$$G_{xy}(f) = H(f)\, G_{xx}(f) \tag{3.2}$$

where $H(f)$ = frequency response function,

$G_{xx}(f)$ = power spectrum of $x(t)$,

$G_{yy}(f)$ = power spectrum of $y(t)$,

and $G_{xy}(f)$ = cross-spectrum between $x(t)$ and $y(t)$.

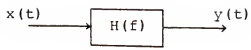

Fig. 3.1. Ideal single input/single output system.

The frequency response function and the coherence function will be introduced in a more realistic model where extraneous measurement noise exists at both input and output points. Let the true signals be u(t) and v(t), and the noise terms be m(t) and n(t), respectively, as shown in Fig. 3.2.

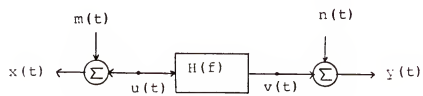

Fig. 3.2. Single input/single output system with extraneous noise.

3.2.1. Frequency Response Function

By assuming that the extraneous noise terms are uncorrelated with each other and with signals, the cross-spectral terms will be

$$G_{xm}(f) = G_{yn}(f) = G_{mn}(f) = 0 \tag{3.3}$$

In terms of true signals u(t) and v(t), Eqs. (3.1) and (3.2) give

$$G_{vv}(f) = |H(f)|^2 G_{uu}(f) \tag{3.4}$$

$$G_{uv}(f) = H(f)\, G_{uu}(f) \tag{3.5}$$

However, the measured power spectra and cross-spectrum are

$$G_{xx}(f) = G_{uu}(f) + G_{mm}(f) \geq G_{uu}(f) \tag{3.6}$$

$$G_{yy}(f) = G_{vv}(f) + G_{nn}(f) \geq G_{vv}(f) \tag{3.7}$$

$$G_{xy}(f) = G_{uv}(f) \tag{3.8}$$

since $G_{mm}(f) \geq 0$ and $G_{nn}(f) \geq 0$ for all f.

Substitution of Eqs. (3.6) and (3.8) into Eq. (3.2) gives

$$\hat{H}(f) = \frac{G_{uv}}{G_{uu} + G_{mm}} = H(f)\left[\frac{1}{1 + (G_{mm}/G_{uu})}\right] \tag{3.9}$$

where "^" indicates "estimate of."

Equation (3.9) shows that an unbiased estimate of the frequency response function can be made, regardless of the value of output noise, when $G_{mm} \ll G_{uu}$, which will nearly always be the case in practice.

However, substitution of EQ. (3.6) and (3.7) into Eq. (3.1) gives

$$|\hat{H}(f)|^2 = |H(f)|^2\left[\frac{1 + (G_{nn}/G_{vv})}{1 + (G_{mm}/G_{uu})}\right] \tag{3.10}$$

Thus even if $G_{mm} \ll G_{uu}$, Eq. (3.10) will always give a biased estimate when $G_{nn} \neq 0$.

In the impulse technique, the frequency response function is obtained by simultaneously measuring and digitally storing the time histories of the structure excitation force and the response signal. These time-domain signals are then used by the Fourier analyzer to calculate, in the frequency domain, the force power spectrum G_{xx}, the response power spectrum G_{yy}, the cross-power spectrum G_{xy}, and the frequency response function H(f), where

$$H(f) = \frac{\overline{G}_{xy}}{\overline{G}_{xx}} \tag{3.11}$$

and "—" indicates average over several samples.

Bendat and Piersol [58] indicate that random error in frequency response function estimates is proportional to $1/\sqrt{2n}$, where n represents number of records or number of averages. Thus through ensemble averaging, the measurement error can be reduced.

3.2.2. Coherence Function

The coherence function is a real-valued quantity defined by

$$\gamma^2_{xy}(f) = \frac{|G_{xy}(f)|^2}{G_{xx}(f)G_{yy}(f)} \tag{3.12}$$

From Eqs. (3.4) through (3.8), the coherence function becomes

$$\gamma_{xy}^2(f) = \frac{G_{uu}(f)G_{vv}(f)}{[G_{uu}(f) + G_{mm}(f)][G_{vv}(f) + G_{nn}(f)]} \leq 1 \qquad (3.13)$$

If extraneous noise is present only at the output point, $G_{mm}(f)$ is equal to zero. Then Eq. (3.13) can be written as

$$\gamma_{xy}^2(f) = \frac{G_{vv}(f)}{G_{vv}(f) + G_{nn}(f)} = \frac{|H(f)|^2 G_{uu}(f)}{G_{yy}(f)} \qquad (3.14)$$

Equation (3.14) provides a simple interpretation of the coherence function. At a given frequency, the coherence function is the fractional portion of the output spectrum of y(t) which is linearly related to x(t).

In the impulse technique, the Fourier analyzer calculates the coherence function by

$$\gamma_{xy}^2(f) = \frac{|\overline{G}_{xy}|^2}{\overline{G}_{xx}\overline{G}_{yy}}, \quad 0 \leq \gamma_{xy}^2 \leq 1. \qquad (3.15)$$

and random error in coherence function estimates is proportional to $1/\sqrt{n}$ [58]. From Eq. (3.13), if noise occurs in either the input or the output signals, the coherence function begins to drop toward zero. The coherence function ranges from 0.0 to 1.0. The larger the potential measurement noise, the system non-linearity, or the number of possible multiple inputs, the lower the coherence function

will be [59]. Thus the coherence function used here is a measure of the "quality" of the data. A coherence value of unity indicates that the output is completely causally related to the input.

3.3. Experimental Procedures and Improvements

An experimental method of the impulse technique with some improvements to measure material damping was developed. Since the damping value of aluminum is well established [37], a 2024-T3 aluminum alloy specimen was used to calibrate the system. Material damping of E-glass/polyester, graphite/epoxy, Kevlar/epoxy, and Ownes-Corning G4 hybrid composites was then measured.

A schematic set-up of the impulse technique first used in the present investigation is shown in Fig. 3.3. An impulse hammer kit (Model K291A) from Piezotronics, Inc., New York, and a Fast Fourier Transform (FFT) analyzer (Model 5420, Hewlet Packard) were used in this study.

The various materials, as shown in Table 3.1, were chosen for the measurements of material damping under flexural vibration. The specimens were fixed by two aluminum blocks at one end. In the original set-up, an accelerometer screwed to a small highly polished anodized aluminum nut (known as adhesive mounting base) which was glued to the tip of each specimen was used to obtain the output response of the beam specimens. A force transducer is mounted to the

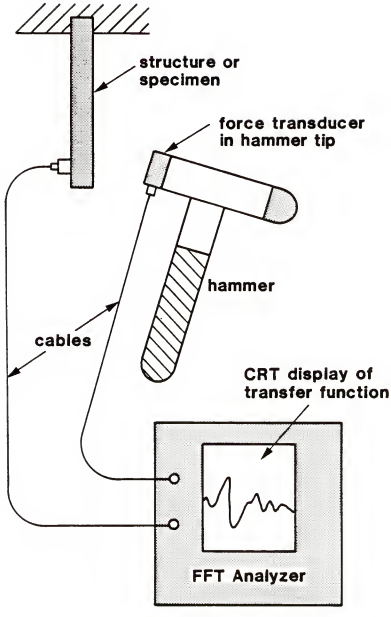

Fig. 3.3. Original schematic drawing of the impulse technique.

Table 3.1: Specimen dimensions.

Specimen	Length (cm)	Width (cm)	Thickness (cm)	Mass (grams)
Aluminum 2024-T3	24.13	1.91	0.32	42.9
E-Glass/Polyester PPG-SMC R65	13.97	2.54	0.28	20.2
Graphite-Epoxy HY-E 1034C $[90_2/0_6/90_2]_S$	24.13	2.54	0.29	28.4
Kevlar/Epoxy HY-E 1734A$_2$ [Unidirectional]	24.38	2.54	0.31	26.75
Hybrid Composite Owens-Corning G4 [O/R/O/R/O]	24.45	3.81	0.45	91.6

Mass of Transducer + Nut + Connector	4.1

head of the hammer which measures the force input to the specimens. The impact point used was near the stiffer portion of the specimen, which was about six centimeters from the fixed end of the specimen in this study. The excitation and response signals were fed into the FFT analyzer which displayed the frequency response function and coherence function. (Both functions were discussed in section 3.2.) For each measurement, the number of ensemble averages was six.

The frequency response function is a complex valued function. A typical experimental display of the real and imaginary parts of H(f) is shown in Fig. 3.4 for graphite/epoxy composite. Stahle and Forlifer [45] give a method to obtain values of resonant frequency and damping from the plot of response curves. Lang [46] applied this method to the measurements of resonant frequency and damping from the displayed response characteristics. The peak of the imaginary part determines the resonant frequency, and then from the corresponding real part (see Fig. 2.3) the material damping, η, can be calculated from the formula [45, 46]

$$\eta = \frac{(f_a/f_b)^2 - 1}{(f_a/f_b)^2 + 1} \tag{3.16}$$

In using the impulse technique to measure the material damping, the following precautions must be taken.

a. It is necessary to avoid measurement of response near nodal points for the modes to be tested.

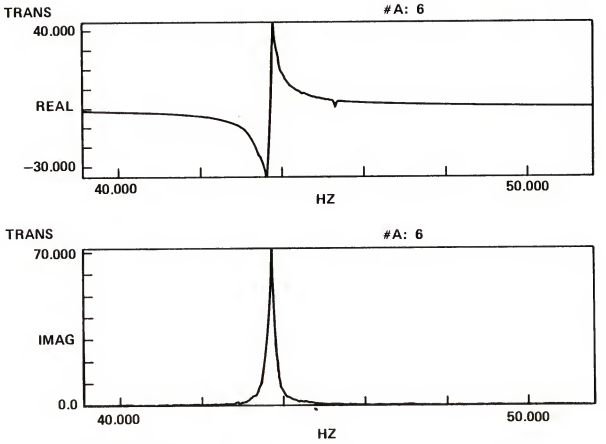

Fig. 3.4. Typical imaginary and real parts of frequency response function.

Such measurements would consist primarily of noise, since the actual response is very small near nodal points.

b. The amplitude of vibration must be kept below the thickness of the specimen to assure that air damping is negligible, since the air damping is linearly proportional to the amplitude-to-thickness ratio of the beam specimen [50].

c. It is important to optimize the Analog to Digital Converter (ADC) range setting on an FFT analyzer before making a measurement, since an optimized ADC range setting will increase resolution in the digitizing process [60].

In the original set-up, an accelerometer added mass to the specimens. This added mass was shown to have a large effect on the natural frequencies of the specimens, and the measured material damping was too high as compared with some well-known results. This observation is especially true for light-weight specimens of composite materials. In order to eliminate the effects of the added mass, a non-contact probe (KD-2310-3U, Kaman Sciences Corp. Colorado), known as a motion transducer, was used. The motion transducer, which is placed about 1.5 mm (0.059 in) below the tip of each specimen, operates under the principle of eddy current. An aluminum foil target of diameter 20 mm (0.787 in) was cemented underneath the tip of the specimen. A schematic drawing of the modified experimental set-up is shown in Fig. 3.5 and a

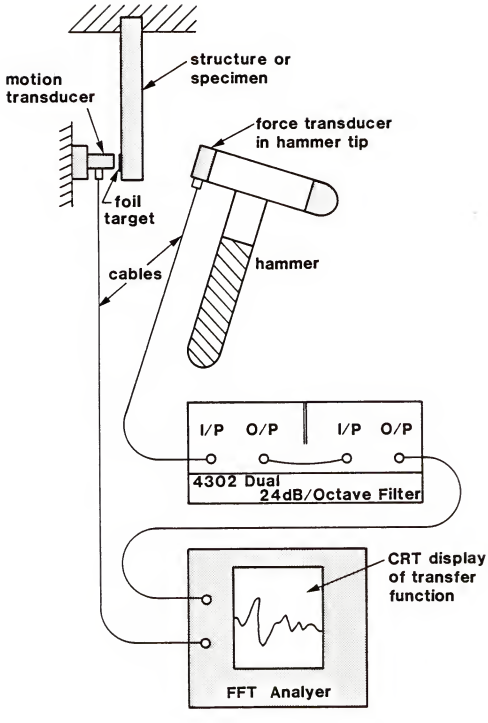

Fig. 3.5. Schematic drawing of the modified impulse hammer experimental set-up.

photographic overview is shown in Fig. 3.6. It is believed that the replacement of a contact accelerometer by a non-contact motion transducer is a major improvement of the impulse hammer technique.

The response signal (which is proportional to ω^2 in a harmonic vibration) from a contact accelerometer probe is much stronger than the response signal from a non-contact displacement probe. Therefore, the coherence between input and output signals by using the non-contact probe is not as good as is obtained using the contact probe. In general, the larger the potential measurement noise, the system nonlinearity, or the number of possible multiple inputs, the lower the coherence function will be. The coherence problem in using the non-contact probe is primarily attributed to the low signal-to-noise ratio. The difference in coherence between contact and non-contact probes can clearly be observed in Fig. 3.7.

In order to improve the coherence, an octave filter (4302 dual 24 db, Ithaco, Inc., New York), which was connected to the force transducer in the hammer tip on one end and to the FFT analyzer on the other end, was introduced as shown in Fig. 3.5. By using this filter, the input signal can be magnified 100 times. A comparison of coherence and transfer functions with and without the filter is shown in Figs. 3.8 and 3.9. Obviously, the coherence value is improved. The effect of interference by the noise level on the magnitude of the transfer function (Fig. 3.9) is

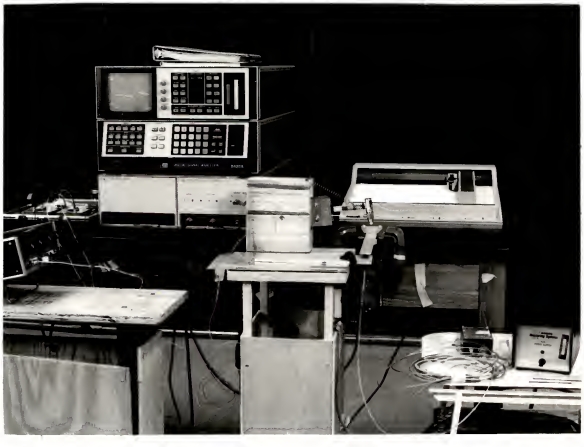

Fig. 3.6. A photographic view of the experimental set-up.

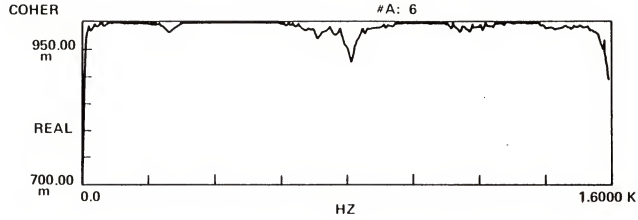

A. Coherence of Graphite/Epoxy Composite (Contact)

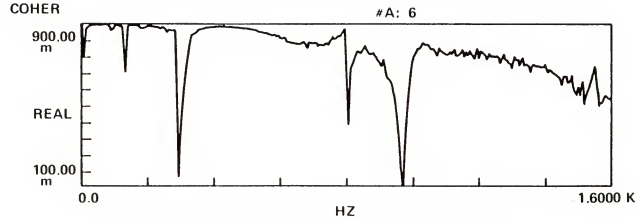

B. Coherence of Graphite/Epoxy Composite (Non-Contact)

Fig. 3.7. Comparison of coherence with contact and non-contact probes.

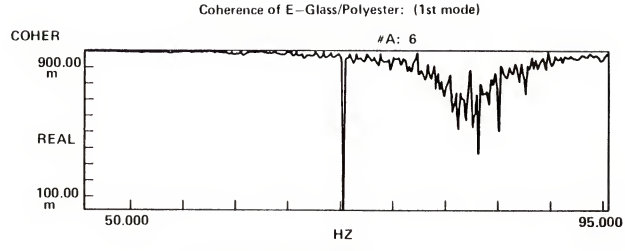

Fig. 3.8. Comparison of coherence with and without amplifier.

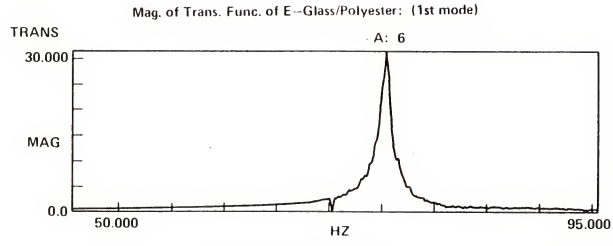

A. Hammer Signal Amplified

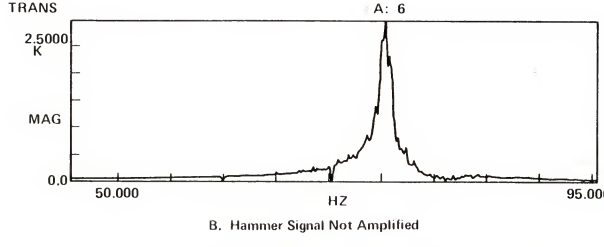

B. Hammer Signal Not Amplified

Fig. 3.9. Comparison of transfer function with and without amplifier.

particularly important when the technique of half-power point is used to measure damping.

After an amplifier is introduced, the following additional problems still exist:

a. The exact location of the impulse of the hammer on the specimen and the force level cannot be accurately controlled.

b. Measured data sometimes are several orders of magnitude higher than the well-known existing data.

In order to further improve the experimental technique, the following steps were taken into consideration:

1. The hammer is connected to a fixed spring so that the magnitude, location and the dwelling time of the impact load can be controlled. The detailed set-up is shown in Fig. 3.10. A comparison of the experimental display of the transfer function and coherence function is shown in Figs. 3.11 and 3.12. In Figs. 3.11 and 3.12, the imaginary part of the transfer function and the coherence function are presented with and without the control by the spring. It is clearly indicated that the resolution and coherence are indeed improved by using a spring to control the impulse characteristics.

2. In order to improve the accuracy of the experimental data of damping associated with a particular mode of vibration, the values of natural frequencies within

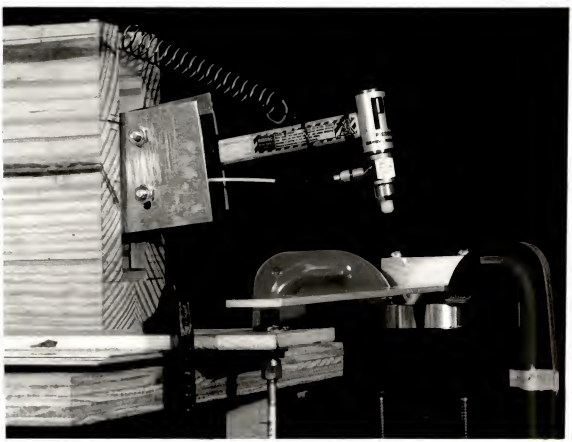

Fig. 3.10. Photographic view of spring attached to the hammer.

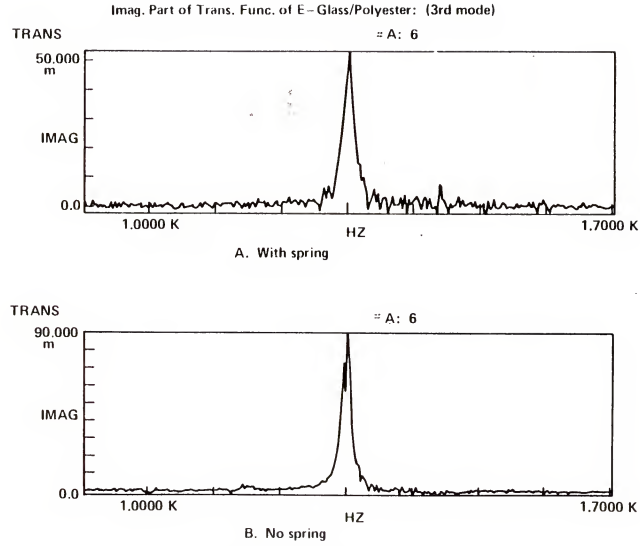

Fig. 3.11. Imaginary part of the transfer function with and without spring control.

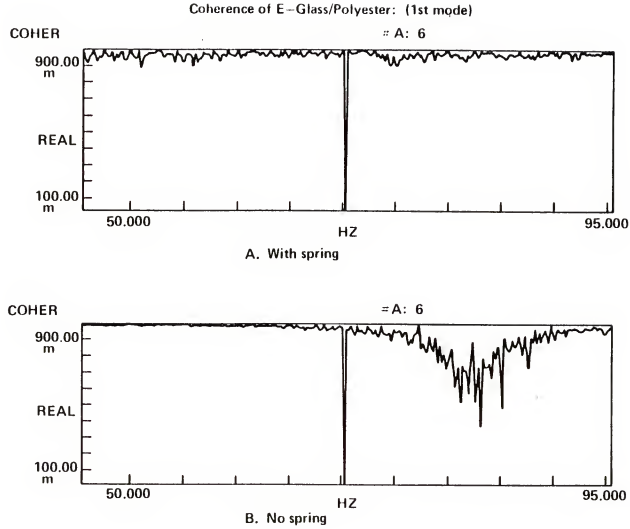

Fig. 3.12. Coherence function with and without spring control.

the frequency range of interest (say from 0 to 1,600 Hz) were first determined approximately. Then a zooming technique to increase the resolution of the response in the neighborhood of this particular frequency was used. By using this technique, the experimental data of material damping of aluminum alloy and some other composites can be obtained, which compare closely with values documented in existing literature.

3.4. Experimental Results and Discussion

The replacement of a contact accelerometer probe by a non-contact displacement transducer is an important step to improve the accuracy of the experimental results. A comparison between the experimental results with contact and non-contact probes is shown in Table 3.2 for five different specimens and the first three fundamental modes of vibrations. Table 3.2 shows consistently that the results with the accelerometer contact probe differ significantly from those obtained with the non-contact probe even though the ratio of the mass of the transducer to the mass of the specimen is as low as 0.045 in the hybrid composite case.

The zooming technique has been shown to improve the experimental data considerably, but it has a certain limitation on the frequency band-width of the measurement. This situation is particularly true for the higher modes. The

Table 3.2: Comparison of experimental results with contact and non-contact probes.

Specimen	Mode	Non-Contact	Contact
		$\eta \times 10^4$	$\eta \times 10^4$
Aluminum 2024-T3	1st	14.33	33.61
	2nd	3.28	7.65
	3rd	2.46	2.83
E-Glass/Polyester PPG-SMC R65	1st	77.83	204.1
	2nd	100.22	155.6
	3rd	71.79	178.5
Graphite/Epoxy HY-E 1034C $[90_2/0_6/90_2]_S$	1st	33.85	52.9
	2nd	40.83	61.5
	3rd	31.32	33.3
Kevlar/Epoxy HY-E 1734 A2 [Unidirectional]	1st	43.59	62.5
	2nd	44.36	50.7
	3rd	31.95	53.4
Hybrid Composite Owens-Corning G4 [O/R/O/R/O]	1st	32.86	46.8
	2nd	42.16	59.8
	3rd	40.47	65.3

experimental results of each kind of specimen are presented in Table 3.3 for the first three modes. In the last column of Table 3.3, BW represents the frequency band width used in each experiment. For each material the value of damping appearing in the first row corresponds to the first mode, and the second row corresponds to the second mode, etc. Table 3.3 shows clearly that the experimental data of damping obtained from base-band measurement (dc to selected frequency ranges) are several orders of magnitude, in some cases, greater than that obtained using zooming measurement. It is also observed from Table 3.3 that the band width chosen for use with the higher modes is relatively large. The reason for this choice is that at higher modes of vibration, the displacement (of the response signal) is small and the effect of noise level becomes important. With a small band width, it was found to be more difficult to resolve the higher-mode signal from the noise than with a broad band width. In this research, the measurements of material damping are up to the third mode. For modes higher than the third, the damping measurements would consist primarily of noise because noise dominates in higher modes of vibration.

After taking into account all the improvements mentioned in section 3.3, the damping values for each material are presented in Table 3.4 and are compared there with existing values for aluminum and E-glass/polyester materials. Each value in Table 3.4 was determined by the smallest value among at least three measurements because the higher damping

Table 3.3: Comparison of experimental results using Base-band and Zoom measurement.

Specimen	Base-band Measurement (0-1.6 KHz)	Zoom Measurement	
	$\eta \times 10^4$	$\eta \times 10^4$	BW (Hz)
Aluminum 2024-T3	1529.4	14.33	8
	229.9	3.28	25
	83	2.46	50
E-Glass/Polyester PPG-SMC R65	798.7	77.83	50
	266.6	100.22	400
	96.2	71.79	800
Graphite-Epoxy HY-E 1034C $[90_2/0_6/90_2]_S$	1529.4	33.85	12.5
	219.8	40.83	100
	78.4	31.32	200
Kevlar/Epoxy HY-E 1734 A_2 [Unidirectional]	1172.4	43.59	12.5
	176.9	44.36	100
	--	31.95	400
Hybrid Composite Owens-Corning G4 [O/R/O/R/O]	1327.4	32.86	12.5
	224.7	42.16	100
	161.3	40.47	400

Table 3.4: Final experimental results.

	Loss Factor, $\eta \times 10^4$ (1st Mode)		
Specimen	Signal Amplified	Not Amplified	Existing Values*
Aluminum (43 Hz) 2024-T3	14.33	14.34	10.5
E-Glass/Polyester (75 Hz) PPG-SMC R65	77.83	103.46	90.0
Graphite/Epoxy HY-E 1034C (43 Hz) $[90_2/0_6/90_2]_S$	33.85	33.85	--
Kevlar/Epoxy HY-E 1734 A_2 (56 Hz) [Unidirectional]	43.59	42.92	--
Hybrid Composite Owens-Corning G4 (45 Hz) [O/R/O/R/O]	32.86	41.93	--

*Refer to reference No. 61.

Table 3.4--continued

	Loss Factor, $\eta \times 10^4$ (2nd Mode)		
Specimen	Signal Amplified	Not Amplified	Existing Values*
Aluminum (275 Hz) 2024-T3	3.28	3.29	3.0
E-Glass/Polyester (467 Hz) PPG-SMC R65	100.22	100.55	98.0
Graphite/Epoxy HY-E 1034C (287 Hz) $[90_2/0_6/90_2]_S$	40.83	40.83	--
Kevlar-Epoxy HY-E 1734 A_2 (354 Hz) [Unidirectional]	44.36	44.42	--
Hybrid Composite Owens-Corning G4 (277 Hz) [O/R/O/R/O]	42.16	42.22	--

*Refer to reference No. 61.

Table 3.4--continued

Specimen	Loss Factor, $\eta \times 10^4$ (3rd Mode)		
	Signal Amplified	Not Amplified	Existing Values*
Aluminum (771 Hz) 2024-T3	2.46	2.46	2.3
E-Glass/Polyester (1296 Hz) PPG-SMC R65	71.79	71.88	99.0
Graphite/Epoxy HY-E 1034C (794 Hz) $[90_2/0_6/90_2]_S$	31.32	39.04	--
Kevlar/Epoxy HY-E 1734 A_2 (976 Hz) [Unidirectional]	31.95	32.16	--
Hybrid Composite Owens-Corning G4 (773 Hz) [O/R/O/R/O]	40.47	40.47	--

*Refer to reference No. 61

values were attributed to the extraneous noise. In general, there are no differences in the results between the damping values with and without the amplifier. However, the coherence values are improved with the amplifier as is shown in Fig. 3.8. During the test, the coherence values obtained after ensemble averaging were greater than 0.85 which indicates an acceptable measurement. Note that the impact point of the hammer on the specimen should be near the stiffer portion of the specimen to obtain the better coherence values. The deviation of the experimental results from existing values in the literature may be attributed to the different fabrication processes of the specimens. Specifically, in the curing cycle, the temperature and pressure may be varied slightly.

Based on the experimental technique developed in this chapter, the evaluation of damage by damping measurements and behavior of damping due to damage will be discussed in the next chapter.

CHAPTER 4
EVALUATION OF DAMAGE BY DAMPING MEASUREMENTS

4.1. Introduction

The purpose of this chapter is to assess the ability of damping measurements to determine the damage state. The technique of measurement of material damping developed in Chapter 3 was employed in this chapter for data acquisition. It will be shown that damping has the advantage of being far more sensitive to damage than resonant frequency is.

The experimental work was done in two phases. In the first phase, the damage was simulated by milling-machine cuts. The reason for using this kind of damage is that both the severities and positions of the damage can be controlled precisely. The bulk of the work was carried out for this type of damage for the more realistic cases, the damage from three-point bending tests and artificial delaminations were considered in the second phase of the work.

The milling-machine cuts were administered in precise increments using an end mill with a diameter of 0.317 cm (0.125 in). They were made symmetric with respect to the neutral axis of the cross section. The damage created was local. Damping was measured up to the third mode of

vibration for various severities and positions of the local damage. The correlation between the damage and damping was investigated to assess the ability of damping measurements to detect the damage. It will also be shown that the sensitivities of damping to local damage for each mode of vibration depend on the position of the damage. Three types of materials were considered in this study. They were SMC R50 chopped fiber composite, Kevlar/epoxy continuous fiber composite, and hybrid composite G4 containing both randomly oriented chopped glass fibers and oriented continuous glass fibers embedded in a polyester resin. It has been observed that the SMC R50 composite is most sensitive to the local damage in the damping measurements.

In the second phase of the work, two types of artificial delaminations were created. The first type of artificial delamination was created by the insertion of 0.076 mm (0.003 in) thick mylar in two interfaces of $[90_5/0_4/90_5]$ glass/epoxy composite to prevent interlaminar bonding over certain areas.

A unidirectional 8-ply 30.48 x 30.48 cm (12 x 12 in) glass/epoxy plate was fabricated for the creation of the second type of delamination. Ten specimens, 25.4 x 2.54 cm (10 x 1 in), were cut from the plate. Glue was applied only to part of the specimen face. By gluing each pair of the specimens face to face, the second type of artificial delamination is the unglued portion of the specimens. This

created delamination areas in the middle plane of the 16-ply unidirectional glass/epoxy composite.

Damage from the three-point bending tests on $[90_2/0_{10}/90_2]$ glass/epoxy composite was obtained by tests performed with a Tinius Olsen testing machine. The ability of damping measurements to detect the damage that resulted from the three-point bending tests and the artificial delaminations was investigated.

In this chapter, the main emphasis is focused on the ability of damping measurements to detect the damage. The experimental work carried out in this chapter was also used to develop a method described in Chapter 5 to roughly locate and quantify the damage from the measured damping values.

4.2 Sensitivities of Damping and Resonant Frequency to Local Damage

Both damping and resonant frequency have the same advantage to be measurable at a single point on the structure and to be independent of the position chosen. The sensitivities of these two properties of the structure to the local damage are compared in this section.

An SMC R50 specimen, 13.8 x 2.54 x 0.244 cm (5.43 x 1 x 0.096 in), was used in this study. The severity of the damage is in terms of percent reduction of the total thickness, which is defined as 100 times the ratio of the amount of reduction in thickness to the total thickness of the specimen, $100x\Delta h/h$. First, the damping and resonant frequency

of the first three modes of vibration of the undamaged specimen were measured. Then, these two properties were obtained from the specimen which was damaged by the milling machine at the position of $x/\ell = 0.033$. The damaged beam is shown in Fig. 4.1.

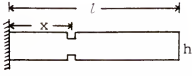

x = position of the damage

ℓ = total length of the specimen

h = total thickness of the specimen

Fig. 4.1. The damaged beam.

The milling-machine cuts were made on the specimen at values of 5, 25, 45, 60, and 70 percent reduction of the total thickness. The experimental results are tabulated for specimen R50-1 in Appendix B.

The following two terms are defined to specify the percent differences from the undamaged values.

$$\text{percent damping difference} = \left|\frac{\eta - \eta_0}{\eta_0}\right| \times 100\% \qquad (4.1)$$

and

$$\text{percent frequency difference} = \left|\frac{\omega - \omega_0}{\omega_0}\right| \times 100\% \qquad (4.2)$$

where η_0 and η are damping of undamaged and damaged specimens, respectively,

and ω_0 and ω are for the case of resonant frequency.

By applying Eqs. (4.1) and (4.2) to the experimental data, the percent damping and frequency differences versus percent reduction of total thickness were determined and plotted for the first three modes of vibration in Figs. (4.2) to (4.4). The curves were fitted by eye to these data.

The experimental results show that damping is far more sensitive to damage than resonant frequency is. This is the reason to choose the damping measurements to evaluate the damage. For the first mode of vibration, the resonant frequency at the highest damage has only changed by 60%, whereas the damping has changed by 97%. For the cases of the second and third modes of vibration, the changes in the damping and resonant frequency are not significant at the damage position of $x/\ell = 0.033$. The sensitivity of the damping depends on the positions of the damage. This topic will be discussed in the next section of this chapter.

It should be noted that there are no differences between the sensitivities of damping and resonant frequency to the damage smaller than 30% reduction of total thickness in this study.

4.3. Behavior of Damping Due to Local Damage

The change in damping of a material due to localized damage is a function of the position and severity of the damage. To evaluate the effects of local damage systematically, milling-machine cuts were made at various known positions on the specimens which were subjected to damping

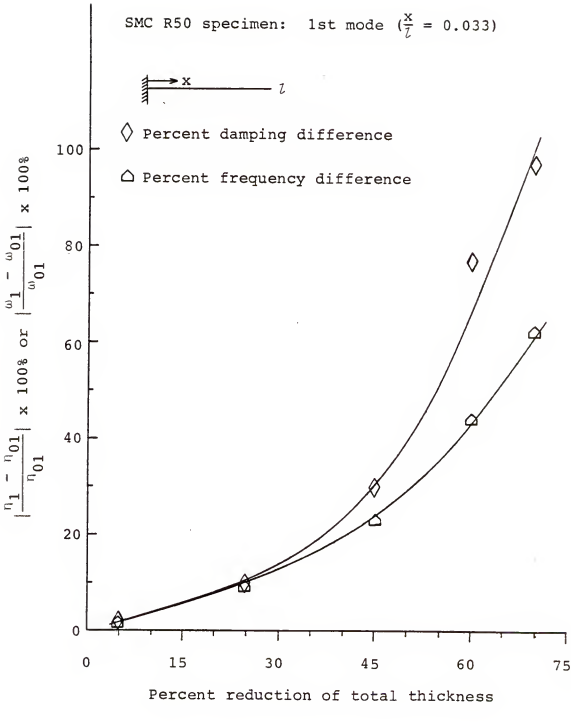

Fig. 4.2. Percent damping and frequency differences between damaged and undamaged conditions vs. severity of the damage--1st mode

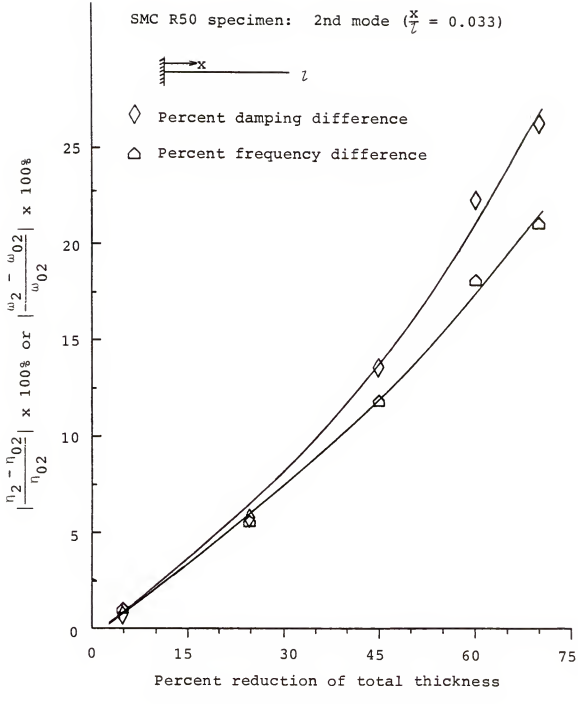

Fig. 4.3. Percent damping and frequency differences between damaged and undamaged conditions vs. severity of the damage--2nd mode

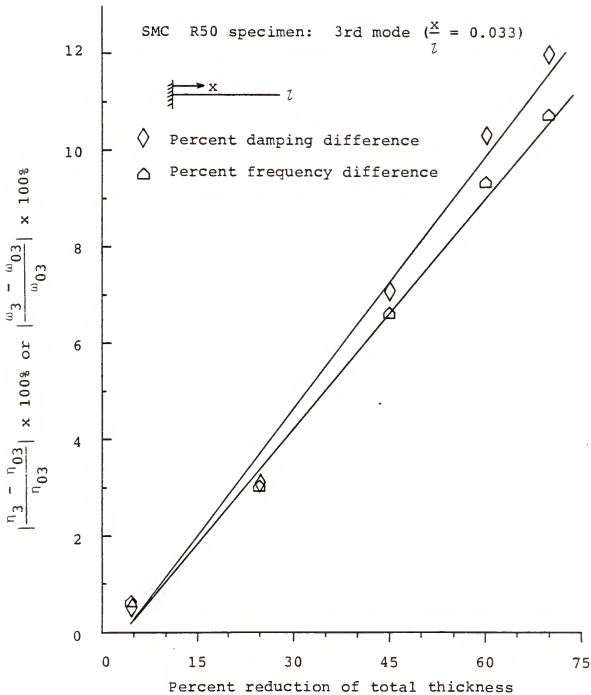

Fig. 4.4. Percent damping and frequency differences between damaged and undamaged conditions vs. severity of the damage--3rd mode

measurements. The results of this procedure are discussed in this section.

Seven positions of the damage are considered in the damping measurements to represent every portion of the specimen. These positions are described as follows:

$x/\ell = 0.033$, close to the root of the beam.

$x/\ell = 0.15$, middle point between $x/\ell = 0.033$ and the first peak of the third mode of vibration.

$x/\ell = 0.3$, the first peak of the third mode of vibration.

$x/\ell = 0.48$, the peak of the second mode of vibration.

$x/\ell = 0.7$, the second peak of the third mode of vibration.

$x/\ell = 0.82$, middle point between the node of the second mode and the second node of the third mode of vibration.

$x/\ell = 0.91$, close to the end of the beam.

Five successive milling machine cuts were made on one specimen for a chosen position of the damage, with damping measurements between successive cuts. These cuts represented 5, 25, 45, 60, and 70 percent reduction of the original thickness.

Only one position of the damage was chosen among the seven positions considered for each specimen. After damping measurements were performed for the undamaged specimens, the damage was made on the specimen at the chosen position. The damping values of the first three modes of vibration of the

damaged specimen were measured after each cut. When the damping measurements were completed for the five cuts at the chosen position, a new specimen was used to carry the measurements beginning with the undamaged state. For the new specimen, the position of the damage was different from that of the previous specimen. This procedure was continued until the damping was measured for each cut at each position of the damage.

The materials investigated were SMC R50 E-glass/polyester, Kevlar/epoxy, and hybrid composite G4. The experimental results are tabulated in Appendices B, C, and D. The correlation between damage and damping and the sensitivity of damping to local damage are discussed in detail under the separate subsections which follow.

4.3.1. Correlation Between Damage and Damping

The loss factors, η, of the SMC R50 material versus percent reduction of total thickness data tabulated in Appendix B are plotted in Figs. 4.5 to 4.10. To clarify the plots, the data obtained at seven positions of damage are divided into two groups. One group includes the data measured at $x/\ell = 0.033$, 0.15, and 0.48. The data obtained at $x/\ell = 0.3$, 0.7, 0.82, and 0.91 are in the other group. Each figure represents data for one group only. Curves have been fitted by eye to these data.

From Figs. 4.5 to 4.10, it is observed that, in general, the severity of the damage correlates well with increased damping for the first three modes of vibration. There are

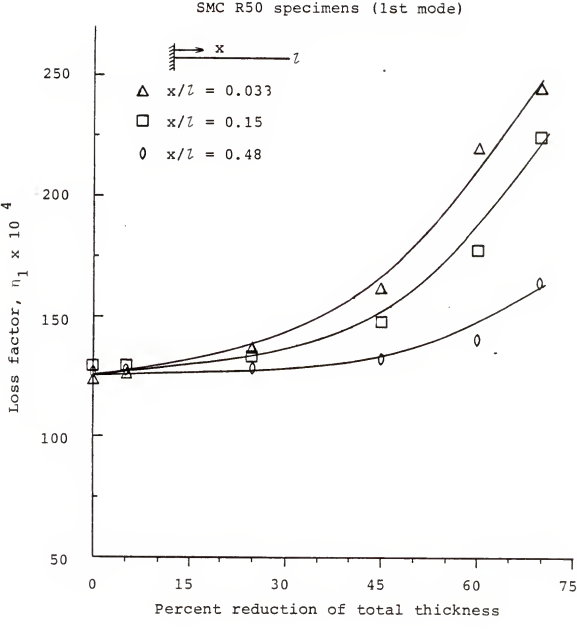

Fig. 4.5. Specimen loss factor vs. severity of damage at x/ℓ = 0.033, 0.15, and 0.48--1st mode

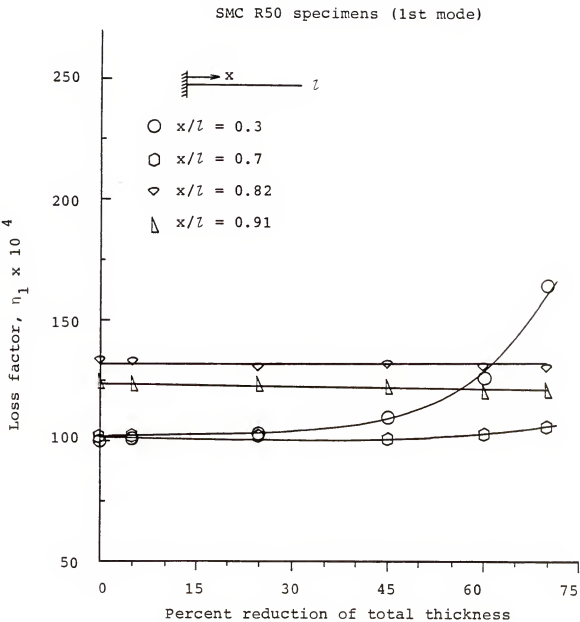

Fig. 4.6. Specimen loss factor vs. severity of damage at x/ℓ = 0.3, 0.7, 0.82, and 0.91--1st mode

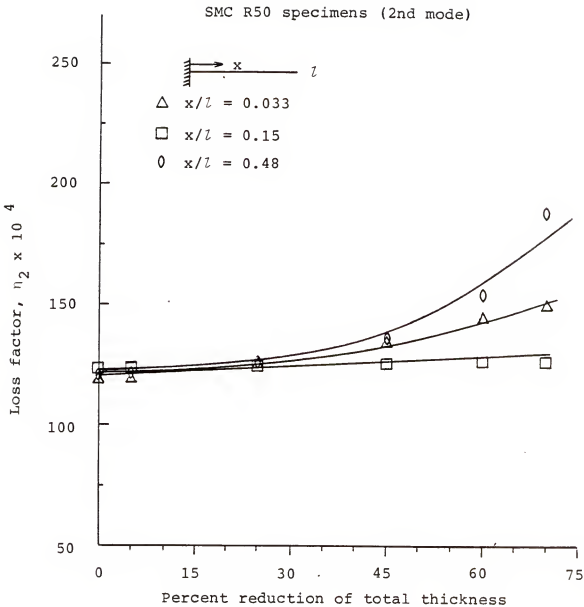

Fig. 4.7. Specimen loss factor vs. severity of damage at x/ℓ = 0.033, 0.15, and 0.48--2nd mode

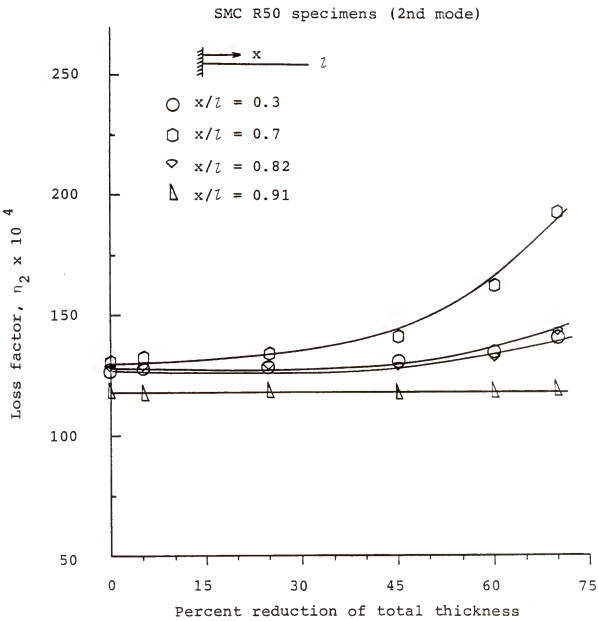

Fig. 4.8. Specimen loss factor vs. severity of damage at x/ℓ = 0.3, 0.7, 0.82, and 0.91--2nd mode

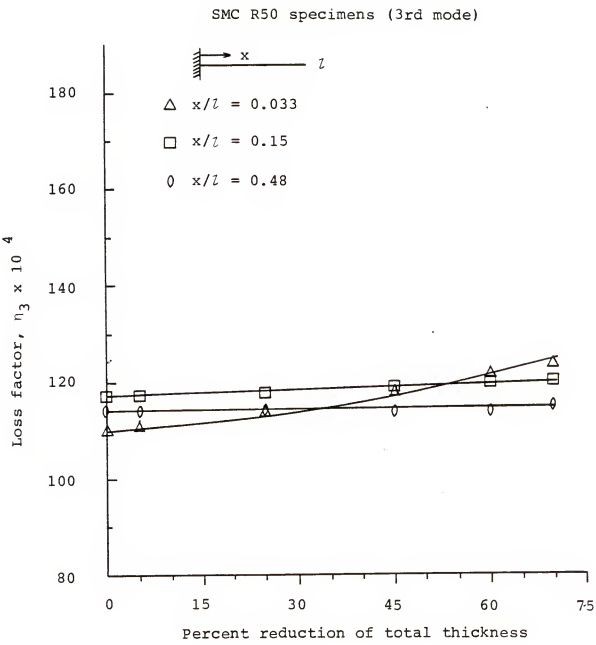

Fig. 4.9. Specimen loss factor vs. severity of damage at $x/\ell = 0.033$, 0.15, and 0.48--3rd mode

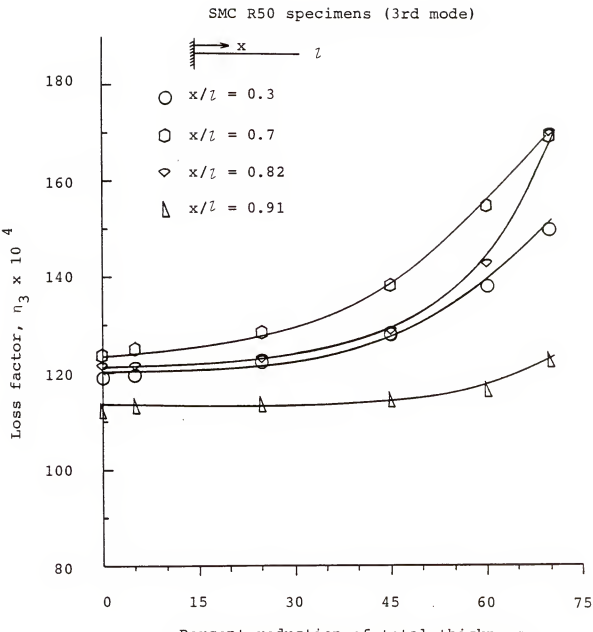

Fig. 4.10. Specimen loss factor vs. severity of damage at x/ℓ = 0.3, 0.7, 0.82, and 0.91--3rd mode

some positions on the specimen at which there is no appreciable change to be expected in damping due to damage. These positions can be observed from Figs. 4.6, 4.8, and 4.9. For the first and second modes of vibration, these positions are near the end of the specimen. For the third mode of vibration, these positions are near the root of the specimen. With this understanding of the behavior of damping in each mode of vibration at various positions of damage, damping measurements can be employed to detect the damage of the materials. However, this technique has some limitation. At less than 5% reduction in total thickness of the specimen, the damage is difficult to detect by the instrument. To detect a small damage, the measurements of higher modes of vibration may be necessary.

From the experimental results of Kevlar-epoxy and hybrid composite materials, the same trends of change in damping due to local damage can be observed as with SMC R50 material.

4.3.2. Sensitivity of Damping to Local Damage

Figures plotted in the previous subsection imply that the change in damping due to local damage depends on the positions of the damage. In applying the technique of damping measurements to detect damage, it is useful to understand the behavior of damping in each mode of vibration at various positions of the damage. A close look at the sensitivity of damping to the presence of the local damage at various positions is considered in this subsection.

The sensitivities of damping of the first three modes of vibration to local damage are compared at each position of the damage. If Eq. (4.1) applies to the experimental data tabulated in Appendices B, C, and D, figures for the percent damping difference versus percent reduction of total thickness can be obtained. Three typical example figures are shown here to get a feeling how the damping of different modes behaves for damage at various positions.

The results of SMC R50 specimen damaged at position $x/\ell = 0.033$ are plotted in Fig. 4.11. This figure shows that the first mode is the most sensitive while the third mode is the least sensitive to the presence of the local damage at $x/\ell = 0.033$.

The results of Kevlar/epoxy and hybrid composite G4 specimens are plotted in Fig. 4.12 and Fig. 4.13, respectively. Figure 4.12 shows that the second mode is the most sensitive while the third mode is the least sensitive to the presence of the local damage at $x/\ell = 0.48$. In Fig. 4.13, the most sensitive is the third mode, and the least sensitive is the first mode at $x/\ell = 0.82$.

It is clear that the sensitivity of damping of each mode to damage depends on the positions. The mode numbers of damping which are the most sensitive to damage at various positions of the damage are listed in Table 4.1 for SMC R50, Kevlar/epoxy, and hybrid composite G4 specimens.

The same trend of sensitivity for each material can be observed in Table 4.1. This indicates that the

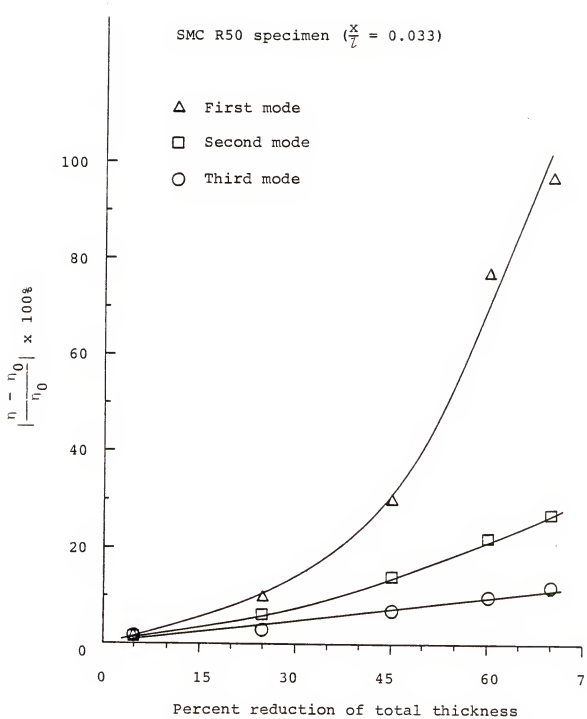

Fig. 4.11. Percent damping difference between damaged and undamaged conditions vs. severity of the damage--SMC R50 specimen

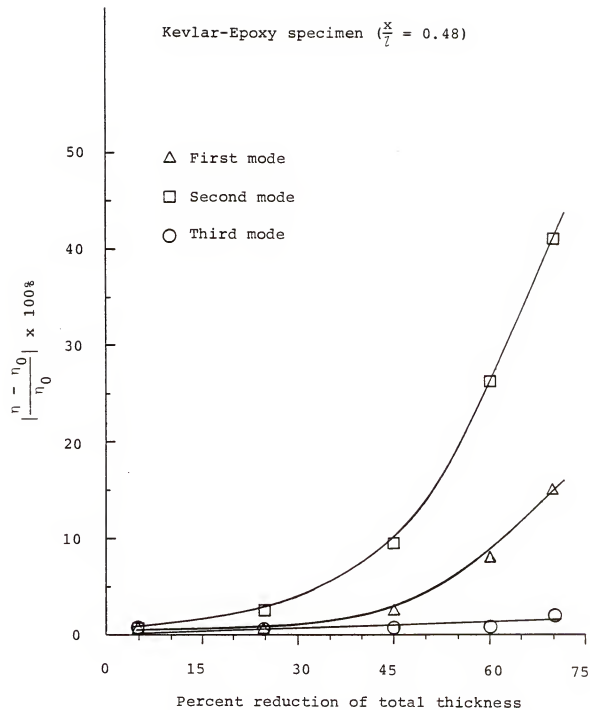

Fig. 4.12. Percent damping difference between damaged and undamaged conditions vs. severity of the damage--Kevlar-epoxy specimen

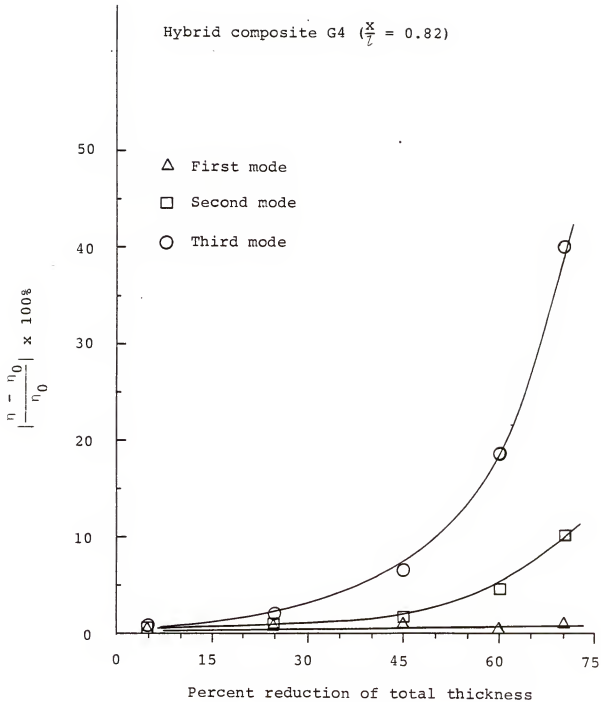

Fig. 4.13. Percent damping difference between damaged and undamaged conditions vs. severity of the damage--hybrid composite G4 specimen

Table 4.1: Mode numbers of damping which are the most sensitive to damage at various positions of the damage.

$\frac{x}{\ell}$	Mode Numbers		
	SMC R50	Kevlar/Epoxy	Hybrid Composite G4
0.033	1	1	1
0.15	1	1	1
0.3	1	1	1
0.48	2	2	2
0.7	3	3	3
0.82	3	--*	3
0.91	3	3	3

*No test in this case.

position-sensitivity of damping due to local damage is independent of the material.

It is also observed that the lower mode is the most sensitive near the root and higher mode is the most sensitive near the end of the specimen. With this understanding, a proper way of damping measurements to detect local damage can be determined.

It is interesting to compare the sensitivities of materials to the presence of local damage. Percent damping differences versus percent reduction of total thickness for SMC R50 and Kevlar/epoxy specimens are plotted in Fig. 4.14. The comparisons between SMC R50 and hybrid composition G4 specimens are plotted in Fig. 4.15.

It is observed that SMC R50 is the most sensitive while Kevlar/epoxy is the least sensitive to the presence of the local damage. The sensitivity of hybrid composite G4 lies in the between. This is reasonable because the hybrid composite G4 contains both randomly oriented chopped glass fibers and oriented continuous glass fibers embedded in a polyester resin. This indicates that the isotropic material is the most sensitive to the presence of the local damage in the damping measurements.

4.4. Studies on Damping Due to Damage from Artificial Delaminations and Three-Point Bending Tests

The change in damping from more realistic cases of damage are investigated in this section to assess the ability of damping measurements to detect the damage.

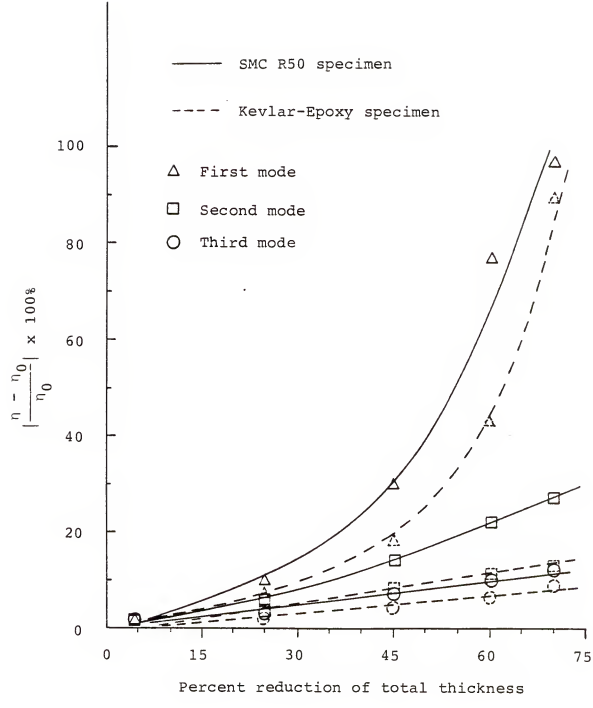

Fig. 4.14. Percent damping difference between damaged and undamaged conditions vs. severity of the damage for SMC R50 and Kevlar-epoxy specimens at $x/\ell = 0.033$

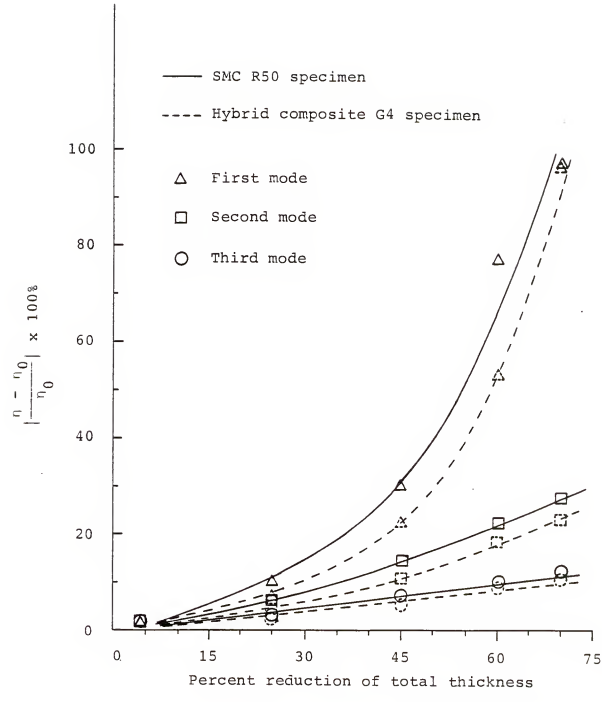

Fig. 4.15. Percent damping difference between damaged and undamaged conditions vs. severity of the damage for SMC R50 and hybrid composite G4 specimens at $x/\ell = 0.033$

Two types of artificial delaminations were created. The first type of artificial delamination was created by the insertion of 0.076 mm (0.003 in) thick mylar in two interfaces of $[90_5/0_4/90_5]$ glass/epoxy composite to prevent inter-laminar bonding over certain areas. The areas of delamination were controlled by various stripes of the rectangular mylar. The layout for artificial delamination inserts in beam specimens is shown in Fig. 4.16. Ten beam specimens were cut from the $[90_5/0_4/90_5]$ glass/epoxy composite plate. During the damping measurements, the beams were clamped at x = 0 as shown in Fig. 4.16.

For the second type of artificial delamination, a unidirectional 8-ply 30.48 x 30.48 cm (12 x 12 in) glass/epoxy plate was fabricated first. Ten specimens, 25.4 x 2.54 cm (10 x 1 in), were then cut from the plate. An undamaged 16-ply composite beam is represented by gluing one pair of specimens face to face completely. For the other specimens, the glue was applied only to part of the specimen faces. By gluing each pair of the specimens face to face, the artificial delamination is represented by the unglued portion of the specimen. The results are four beam specimens which contain the delamination areas in the middle planes of the 16-ply unidirectional glass/epoxy composite. The configurations of the beam specimen and the areas of artificial delaminations are shown in Fig. 4.17. The beams were clamped at x = 0 in the damping measurements.

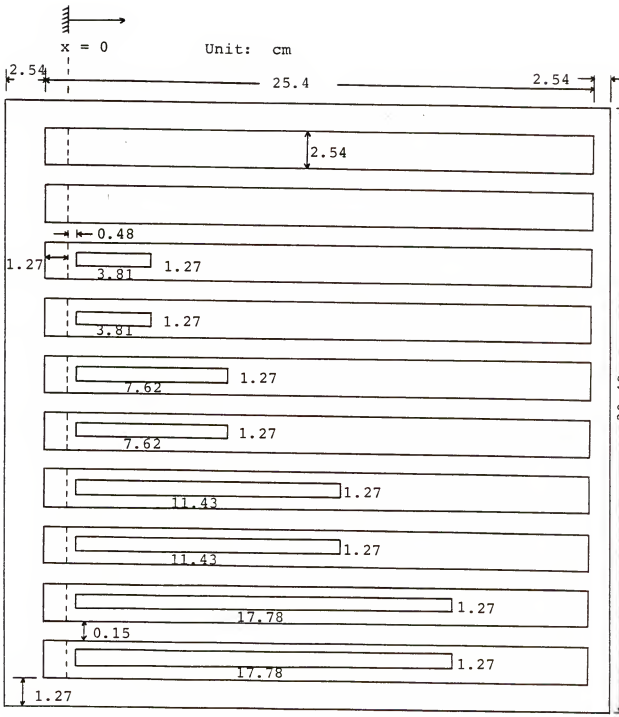

Fig. 4.16. Layout for artificial delamination inserts in two interfaces of $[90_5/0_4/90_5]$ glass/epoxy beam specimens

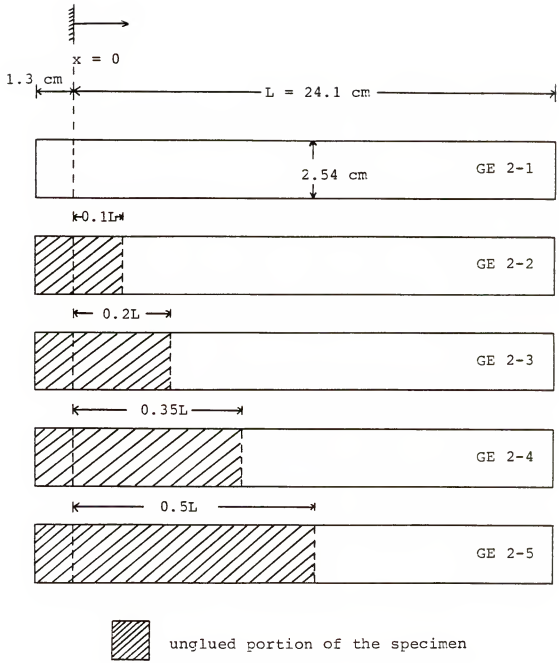

Fig. 4.17. Artificial delaminations represented by the unglued portion in the middle plane of 16-ply unidirectional glass/epoxy specimens

Damage from the three-point bending tests was obtained from tests performed by a Tinius Olsen testing machine. Six specimens, 25.4 x 2.54 cm (10 x 1 in), were cut from a $[90_2/0_{10}/90_2]$ glass/epoxy composite plate. During the damping measurements, the beams were clamped at 7.4 cm (2.91 in) from the left end of the specimens.

At first, in the three-point bending tests, one specimen was used to determine maximum load, P_{max}, that could be carried by the beam. The specimen was centrally loaded at $x/\ell = 0.3$ by a wedge with a rounded edge. The span between the supports is three inches. The loading history was traced on the chart by the machine. The maximum load was determined as $P_{max} = 260$ lb from the chart.

Damping measurements were performed for each specimen in the undamaged state. The severities of damage were controlled by various amounts of load in three-point bending tests. Five values of load were chosen. They are 0.3 P_{max}, 0.45 P_{max}, 0.7 P_{max}, 0.9 P_{max}, and 1.0 P_{max}. There is only one load applied for each specimen. The damping measurements were performed after each load was applied to the specimen.

The experimental results of damping measurements of the three kinds of specimens, i.e., specimens with artificial delamination inserts, unglued type of artificial delaminations, and damage from three-point bending tests are summarized in Tables 4.2, 4.3, and 4.4, respectively.

Table 4.2: Results of damping measurements of $[90_5/0_4/90_5]$ glass/epoxy specimens with inserts to represent artificial delaminations.

Specimen Number	Artificial Delamination Area, cm^2	Damping			$\left\lvert \left(\frac{\eta_i - \eta_{0i}}{\eta_{0i}}\right) \times 100\% \right\rvert$		
		$\eta_1 \times 10^4$	$\eta_2 \times 10^4$	$\eta_3 \times 10^4$	i = 1	i = 2	i = 3
GE 1-1	0	27.865	27.81	39.776			
GE 1-2	0	28.67	28.526	40.668			
Average		28.268	28.168	40.222			
GE 1-3	9.68	27.133	27.094	39.076			
GE 1-4	9.68	27.769	27.657	39.776			
Average		27.451	27.376	39.426	2.9%	2.8%	2%
GE 1-5	19.36	26.559	26.983	38.773			
GE 1-6	19.36	26.631	27.02	38.946			
Average		26.595	27.002	38.86	5.9%	4.1%	3.4%
GE 1-7	29.03	26.348	26.66	38.548			
GE 1-8	29.03	26.348	26.66	38.474			
Average		26.348	26.66	38.511	6.8%	5.4%	4.3%
GE 1-9	45.16	26.383	26.732	38.946			
GE 1-10	45.16	28.039	27.617	40.177			
Average		27.211	27.175	39.562	3.7%	3.5%	1.6%

Table 4.3: Results of damping measurements of 16-ply unidirectional glass/epoxy specimens with unglued area to represent artificial delaminations.

Specimen Number	Artificial Delamination		Damping			$\lvert(\frac{\eta_i - \eta_{0i}}{\eta_{0i}}) \times 100\%\rvert$		
	Length (L=24.1 cm)	Area (cm^2)	$\eta_1 \times 10^4$	$\eta_2 \times 10^4$	$\eta_3 \times 10^4$	i=1	i=2	i=3
GE 2-1	0	0	23.454	29.847	42.666			
GE 2-2	0.1L	6.12	23.149	29.67	43.266	1.3%	0.6%	1.4%
GE 2-3	0.2L	12.24	23.752	32.206	48.466	1.3%	7.9%	13.6%
GE 2-4	0.35L	21.43	24.138	39.076	52.303	2.9%	30.9%	22.6%
GE 2-5	0.5L	30.61	25.309	42.486	55.313	7.9%	42.3%	29.6%

Table 4.4: Results of damping measurements of $[90_2/0_{10}/90_2]$ glass/epoxy specimens with damage due to three-point bending tests.

Specimen Number	Load in 3-Point Bending Test	Damping			$\lvert(\frac{\eta_i - \eta_{0i}}{\eta_{0i}}) \times 100\%\rvert$		
		$\eta_1 \times 10^4$	$\eta_2 \times 10^4$	$\eta_3 \times 10^4$	i = 1	i = 2	i = 3
GE 3-1	0	28.878	24.501	35.155			
	0.3 P_{max}*	28.792	24.561	35.404	0.3%	0.2%	0.7%
GE 3-2	0	27.699	23.715	34.184			
	0.45 P_{max}	28.01	23.885	34.427	1.1%	0.7%	0.7%
GE 3-3	0	26.148	23.193	33.221			
	0.7 P_{max}	26.853	23.437	33.959	2.7%	1.1%	2.2%
GE 3-4	0	27.966	23.8	34.133			
	0.9 P_{max}	28.436	24.116	34.848	1.7%	1.3%	2.1%
GE 3-5	0	28.097	23.971	34.427			
	1.0 P_{max}	28.934	24.351	35.155	3%	1.6%	2.1%

*P_{max} = 260 lb

The averaged values in the first row of Table 4.2 are the damping of the specimen in the undamaged state. The last three columns represent the percent damping differences between damaged and undamaged conditions for the first three modes of vibration. They indicate no significant change in the damping of the specimens having inserts to represent the artificial delamination. This lack of expected damping enhancement is attributed to the following factors which affect the material damping associated with each specimen to the extent that the relatively small change in damping due to inserts may be masked.

A. Due to high pressure and temperature, in the process of fabrication of the specimens, the inserts are bonded with the materials. This results in less friction between the interfaces.

B. Material damping variation between the specimens due to nonhomogeneity (excluding inserts) may be more than that due to inserts.

C. The variation in damping due to clamping at the mounting base may be more than the damping change caused by the mylar inserts.

Therefore, the delamination damage that is simulated by embedding artificial inserts at two interfaces of $[90_5/0_4/90_5]$ glass/epoxy composite specimens cannot be detected by the damping measurements.

Factor A above can be improved by increasing the friction in the delaminated area. Sixteen-ply unidirectional

glass/epoxy specimens with unglued area in the middle plane were made for this purpose. The results of damping measurements for this type of artificial delamination are presented in Table 4.3. Obviously, the significant change can be observed from the second and the third modes. The second mode is the most sensitive to the presence of this type of damage. The severity of the damage correlates well with increased damping. Thus, the technique of damping measurements can be employed to detect the delamination damage that is simulated by unglued area in the middle plane of 16-ply unidirectional glass/epoxy specimens.

The results of damping measurements of $[90_2/0_{10}/90_2]$ glass/epoxy specimens with damage due to three-point bending tests are presented in Table 4.4. It is observed that no significant change can be expected. The damage due to three-point bending tests is mainly of the matrix-crack type. In small amplitude (less than 3 mm) of vibration, energy losses due to friction within the matrix crack may be small as compared to the material damping variation between the specimens due to nonhomogeneity and to the losses occurring at the mounting base due to clamping of the specimens. It is also possible that, in this type of loading, very little damage occurs until the maximum load is approached closely.

The main emphasis has been focused on the ability of damping measurements to detect the damage. A graphic method, which resulted from the experimental work, will be introduced

in the next chapter to roughly locate and quantify the damage from the measured damping values.

CHAPTER 5
METHOD OF LOCATION AND SEVERITY OF DAMAGE

5.1. Introduction

The location and severity of damage are the most important information to know, once the damage is detected. It has been shown that the change in damping of a material due to localized damage is a function of the position and severity of the damage. If percent damping differences of the first three modes versus positions of damage for various severities of the damage are plotted, a graphic method is introduced to roughly locate and quantify the damage from the measured damping values.

Evaluation of the method will be made for the materials of SMC R50 chopped fiber composite, Kevlar/epoxy continuous fiber composite, and hybrid composite G4 specimens.

5.2. Description of the Method

To describe the method, an example is given from the damping measurements of an SMC R50 specimen. The percent damping differences of the first three modes calculated from the experimental results tabulated in Appendix B versus positions of damage for various severities of the damage are plotted in Figs. 5.1, 5.2, and 5.3. The main emphasis here

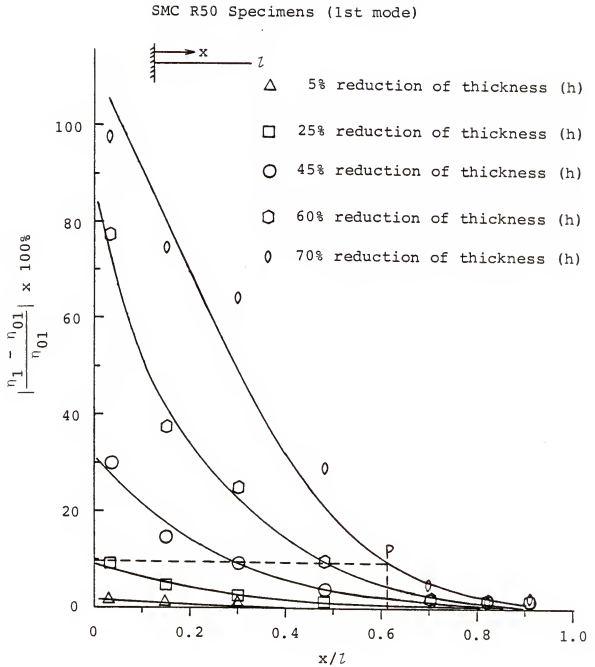

Fig. 5.1. Percent damping difference between damaged and undamaged conditions vs. locations of damage for various severities of the damage--1st mode

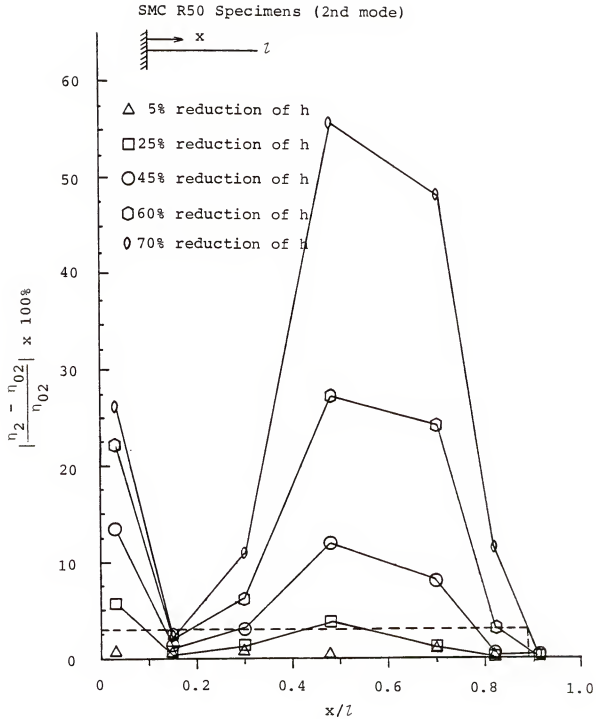

Fig. 5.2. Percent damping difference between damaged and undamaged conditions vs. locations of damage for various severities of the damage--2nd mode

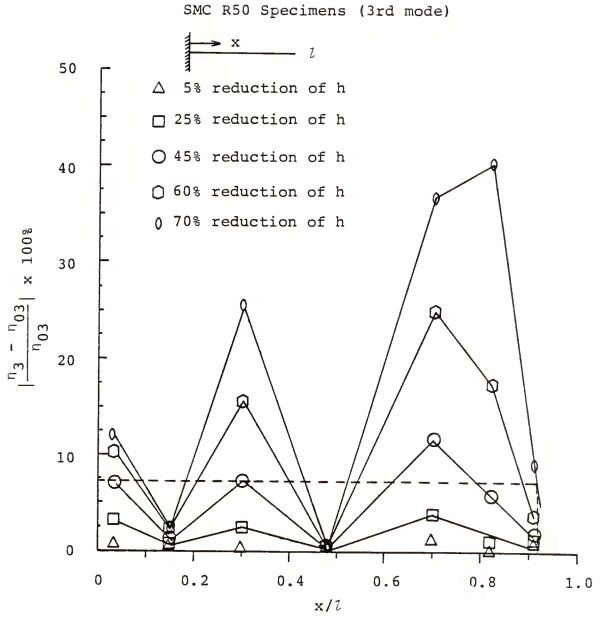

Fig. 5.3. Percent damping difference between damaged and undamaged conditions vs. locations of damage for various severities of the damage--3rd mode

is placed on the procedure of the method. Accuracy can be achieved only with more data points. Thus, curves in Fig. 5.1 are fitted by eye, and straight lines are used to connect data points in Figs. 5.2 and 5.3.

As an example, the calculated percent damping differences from damping measurements at $x/\ell = 0.3$ and 45% reduction in thickness of specimen numbered R50-3 (see Appendix B) are 9.4, 3.0, and 7.3% for the first, second, and third modes, respectively. Now, it is desired to get answers on location and severity of the damage from the known values of percent damping differences. This can be done by using Figs. 5.1, 5.2, and 5.3.

The percent damping difference for the first mode is 9.4%. A horizontal dashed line is drawn to the value of 9.4% as shown in Fig. 5.1. Then, a vertical dashed line is drawn from point P to the x/ℓ axis. This indicates that the possible locations of damage are $x/\ell = 0$ to 0.62. Similarly, the dashed line in Fig. 5.2 indicates that the possible locations of damage are $x/\ell = 0$ to 0.15 and $x/\ell = 0.17$ to 0.9. In Fig. 5.3, the possible locations of damage are shown by the dashed line to be $x/\ell = 0$ to 0.1, $x/\ell = 0.19$ to 0.44, and $x/\ell = 0.51$ to 0.92.

The location of damage evaluated from each mode should refer to the same place. The intersections of all of the possible locations of damage are $x/\ell = 0$ to 0.1, $x/\ell = 0.19$ to 0.44, and $x/\ell = 0.51$ to 0.62. Thus, the possible locations of damage are now limited to the three possibilities.

For each possibility, the possible severities of damage can be evaluated from Figs. 5.1 to 5.3.

For the possibility of $x/\ell = 0$ to 0.1, the possible severities of damage can be evaluated along the dashed line on the interval of $x/\ell = 0$ to 0.1 in Fig. 5.1 as 26% to 30% reduction in total thickness. Similarly, the possible severities of damage are evaluated in Fig. 5.2 as 15% to 25%. In Fig. 5.3, the possible severities of damage are evaluated as 43% to 70%. Again, the intersection is desired from the evaluations of all modes. There is no intersection in this case. Thus, the possibility of $x/\ell = 0$ to 0.1 is not the answer for the location of damage.

For the possibility of $x/\ell = 0.19$ to 0.44, the possible severities of damage are evaluated as 35% to 55% and 22% to 58% from Figs. 5.1 and 5.2, respectively. In Fig. 5.3, the possible severities of damage are evaluated as 45% to 60% and 45% to 70%. The intersection is 45% to 55%.

Finally, for the possibility of $x/\ell = 0.51$ to 0.62, the possible severities of damage are evaluated as 60% to 70%, 22% to 27%, and 45% to 70% from Figs. 5.1, 5.2, and 5.3, respectively. There exists no intersection again.

Obviously, the answers of the example are

location of damage: $x/\ell = 0.19$ to 0.44,

severities of damage: 45% to 55% reduction in total thickness.

The exact answers are $x/\ell = 0.3$ and 45% reduction in total thickness. It is clear that the method gave correct

ranges in evaluations of the location and severity of the damage in this example.

5.3. Evaluation of the Method

For one example given in last section, the method offered correct informations on location and severity of damage. The evaluation of the method will be made for the materials of SMC R50, Kevlar/epoxy, and hybrid composite specimens to further confirm the correctness of the method.

The percent damping differences of the first three modes calculated from the experimental results tabulated in Appendix C versus positions of damage for various severities of the damage are plotted in Figs. 5.4 to 5.6. For hybrid composite G4 specimens, tabulated in Appendix D, the curves are plotted in Figs. 5.7 to 5.9.

The method is applied to each material at data points to evaluate the damage. The results are shown in Tables 5.1, 5.2, and 5.3 for the SMC R50, Kevlar/epoxy, and hybrid composite specimens, respectively.

The percent damping differences, $|(\eta_i - \eta_{0i})/\eta_{0i}| \times 100\%$, in the tables are calculated from the data tabulated in Appendices B, C, and D. Both actual and evaluated values of locations and severities of the damage are listed in the tables for the comparison purpose.

The correctness of the method was checked at data points for each material with the data of Appendices B, C, and D. The method was also checked for some additional arbitrary

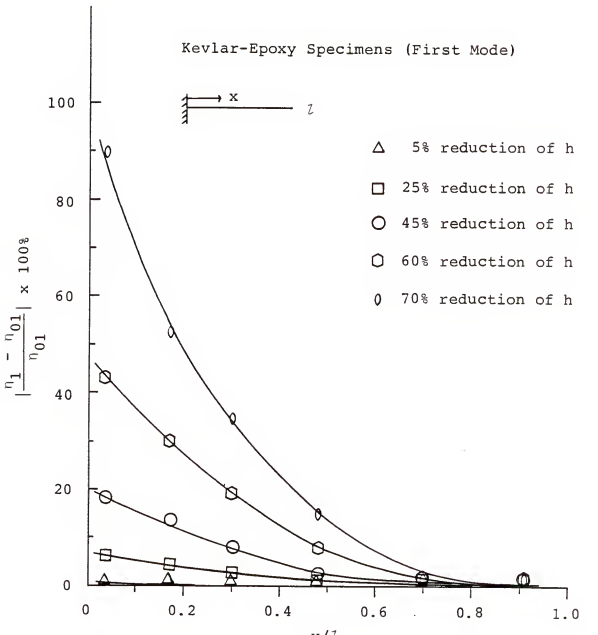

Fig. 5.4. Percent damping difference between damaged and undamaged conditions vs. locations of damage for various severities of the damage--1st mode

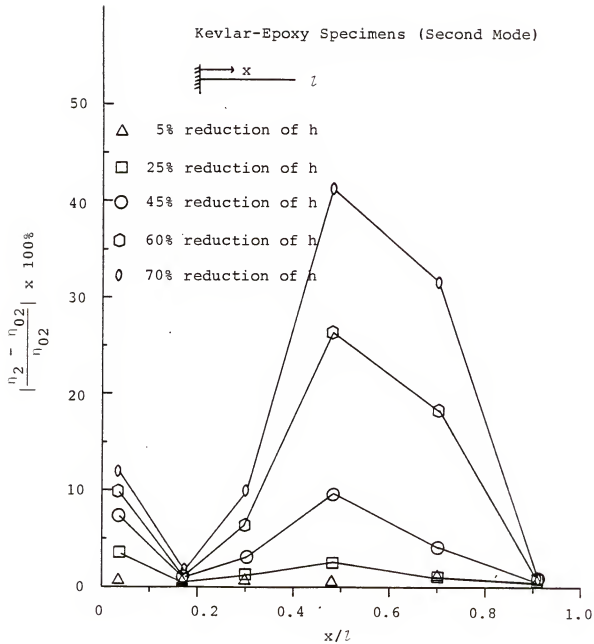

Fig. 5.5. Percent damping difference between damaged and undamaged conditions vs. locations of damage for various severities of the damage--2nd mode

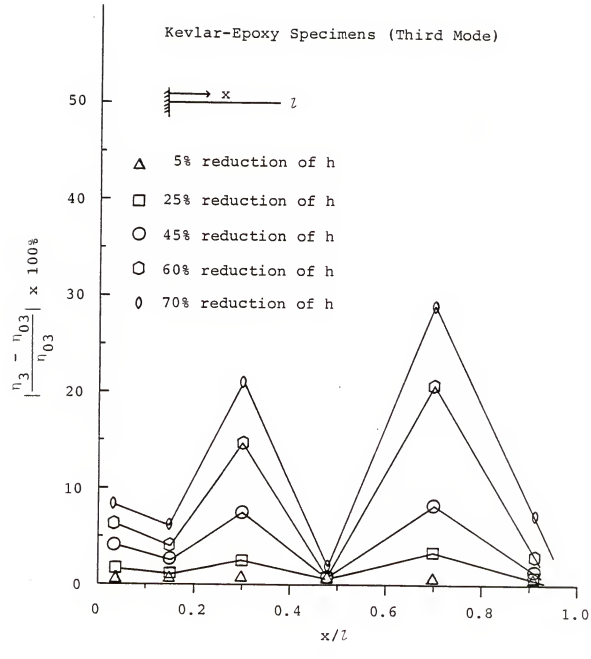

Fig. 5.6. Percent damping difference between damage and undamaged conditions vs. locations of damage for various severities of the damage--3rd mode

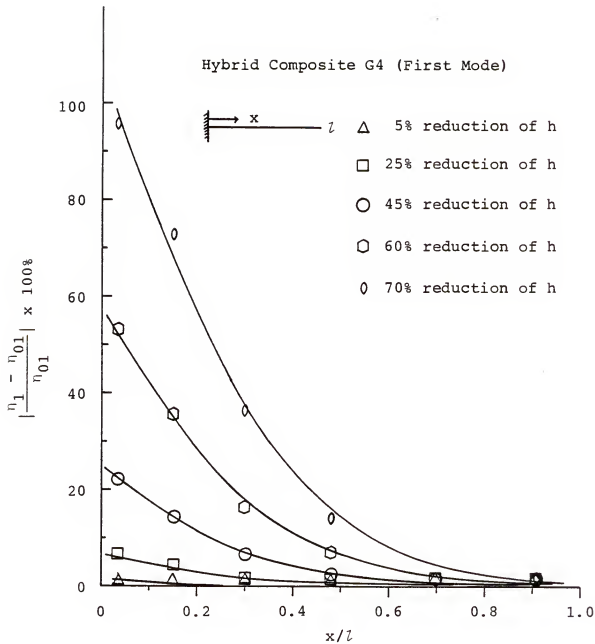

Fig. 5.7. Percent damping difference between damaged and undamaged conditions vs. locations of damage for various severities of the damage--1st mode

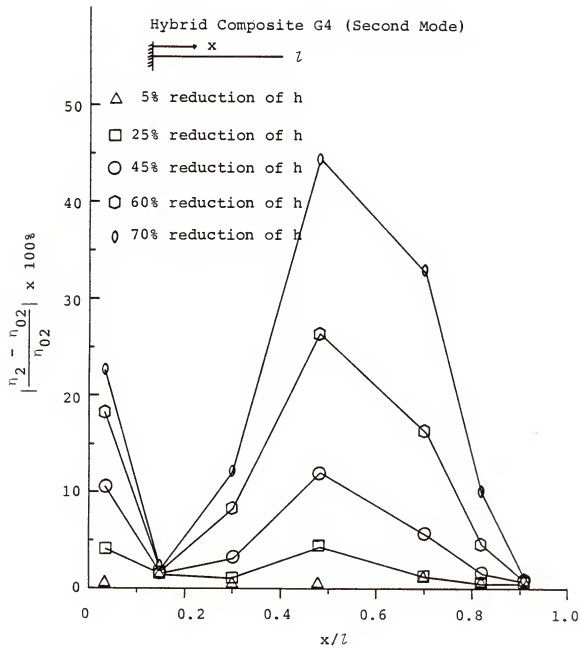

Fig. 5.8. Percent damping difference between damaged and undamaged conditions vs. locations of damage for various severities of the damage--2nd mode

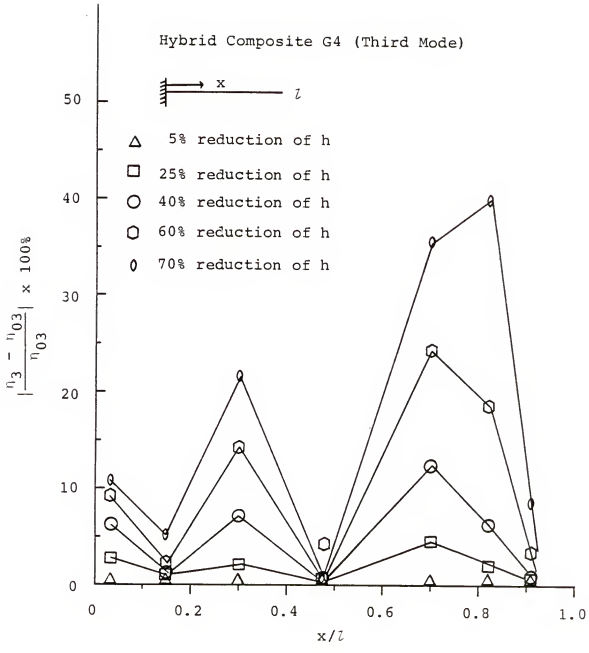

Fig. 5.9. Percent damping difference between damaged and undamaged conditions vs. location of damage for various severities of the damage--3rd mode

Table 5.1: Actual and evaluated positions and severities of damage of SMC R50 specimens.

Specimen			SMC R50			
$\left\|\frac{\eta_i - \eta_{0i}}{\eta_{0i}}\right\| \times 100\%$			Damage positions, $\frac{x}{\ell}$		% reduction of thickness	
i=1	i=2	i=3	Actual	Evaluated	Actual	Evaluated
9.5	5.8	3.1	0.033	(0-0.14)	25%	(25%-30%)
4.5	0.6	0.6	0.15	(0-0.15)	25%	(12%-25%)
2.4	1.2	2.4	0.3	(0.15-0.47)	25%	(25%-35%)
0.9	3.8	0	0.48	(0.17-0.88)	25%	(25%-65%)
0.5	2.4	3.8	0.7	(0.49-0.9)	25%	(25%-60%)
1.6	0	1.2	0.82	(0.49-0.88)	25%	(25%-30%)
0.9	0	1.1	0.91	(0.48-0.91)	25%	(15%-40%)
0.3	3.4	1.5	0.58	(0.49-0.89)	25%	(22%-25%)

Table 5.2: Actual and evaluated positions and severities of damage of Kevlar/epoxy specimens.

Specimen			Kevlar/Epoxy			
$\left\lvert\frac{\eta_i - \eta_{0i}}{\eta_{0i}}\right\rvert$ x 100%			Damage Position, $\frac{x}{\ell}$		% reduction of thickness	
i=1	i=2	i=3	Actual	Evaluated	Actual	Evaluated
18	7.2	4	0.033	(0-0.1)	45%	(45%-47%)
13.5	0.9	2.6	0.15	(0.15-0.47)	45%	(45%-60%)
8	3	7.5	0.3	(0.19-0.43)	45%	(45%-53%)
2.5	9.4	0.5	0.48	(0.48-0.85)	45%	(45%-60%)
0.2	4	8.2	0.7	(0.7-0.9)	45%	(45%-70%)

Table 5.3: Actual and evaluated positions and severities of damage of hybrid composite G4 specimens.

Specimen			Hybrid Composite G4			
$\left\|\frac{\eta_i - \eta_{0i}}{\eta_{0i}}\right\| \times 100\%$			Damage positions, $\frac{x}{\ell}$		% reduction of thickness	
i=1	i=2	i=3	Actual	Evaluated	Actual	Evaluated
22	10.5	6	0.033	(0-0.1)	45%	(43%-48%)
14.2	1.4	1.2	0.15	(0-0.15)	45%	(35%-45%)
6.5	3.1	7	0.3	(0.17-0.43)	45%	(45%-53%)
2.7	11.8	0	0.48	(0.3-0.78)	45%	(45%-65%)
0.2	5.6	12.3	0.7	(0.55-0.86)	45%	(45%-60%)
10.3	0.6	6.9	0.24	(0.17-0.3)	45%	(45%-50%)

locations, i.e., $x/\ell = 0.58$ in Table 5.1 and $x/\ell = 0.24$ in Table 5.3. The severities of damage checked are 25% for the SMC R50 specimen and 45% for the other two specimens.

It is observed that the actual values are within the evaluated ranges. The method has been shown to be valid in the determination of the location and severity of damage. However, the ranges determined are large in the sense of the interval covered. This could be improved with more data points. The number of curves representing the various severities of damage can be increased by offering more data points to narrow down the ranges determined.

It is possible to use the percent reduction of total thickness of specimen to quantify the damage in more realistic case. Two specimens of SMC R50 material were damaged by three-point bending tests. The maximum load of the specimens, P_{max}, was determined as 79 lb. One specimen was loaded at $x/\ell = 0.42$ with loading up to $0.7\ P_{max}$. The other specimen was loaded at $x/\ell = 0.61$ with loading up to $0.8\ P_{max}$. The percent damping differences were calculated from the damping measurements. The location and equivalent percent reduction of total thickness can be evaluated by applying the method to Figs. 5.1 to 5.3. The results are shown in Table 5.4.

The method evaluated correctly the location of the damage. Another valuable information is the equivalent percent reduction of total thickness to the damage created by the bending tests. For example, the table indicates that

Table 5.4: Damage resulted in 3-point bending tests evaluated by equivalent percent reduction of total thickness.

Specimen			SMC R50			
$\left\|\frac{\eta_i - \eta_{0i}}{\eta_{0i}}\right\| \times 100\%$			Damage positions, $\frac{x}{\ell}$		Severities of damage	
					Load in bending test	% reduction of thickness
i=1	i=2	i=3	Position of load	Evaluated	Actual	Evaluated
0.7	0.7	0.3	0.42	(0.15-0.48)	0.7 P_{max}	(5%-20%)
0.6	1.5	0.8	0.61	(0.48-0.7)	0.8 P_{max}	(12%-25%)

the damage made by bending test with 0.8 P_{max} of load is equivalent to 12% to 25% reduction of total thickness.

The percent reduction of total thickness of the specimen can be controlled precisely. Similar figures to Figs. 5.1 to 5.3 of the SMC R50 material can be established for the other materials. Therefore, it is possible to use the method and the percent reduction of total thickness to locate and quantify the damage for more realistic cases. Further work can be done in this area.

CHAPTER 6
SUMMARY AND CONCLUSIONS

6.1. Summary of the Results

The use of the impulse technique for damping measurements to assess the integrity of fiber reinforced composites has been investigated. In damping, the energy of the vibrating system is dissipated as friction or heat. Most damping measurements rely either on decay, resonant dwell, or band width. The relatively new impulse technique was used because of its distinct advantage of being able to generate all higher modes simultaneously.

Several improvements have been made in the impulse technique. These improvements are summarized as follows.

a. A contact probe is replaced by a non-contact probe.
b. An amplifier is used to reduce the noise level.
c. A spring is used to control the magnitude, location and dwell time of the applied force.
d. A zooming technique is used to increase the resolution of the response signal.

More accurate damping data and better coherence values can be obtained after taking into account all the improvements mentioned above. The damping measurements were performed simultaneously for the first three modes of vibration in

this research. For modes higher than the third, the damping measurements would consist primarily of noise because noise dominates in higher modes of vibration.

Based on the impulse technique developed, the evaluation of damage by damping measurements was investigated. Both damping and resonant frequency have the same advantage to be measurable at a single point on the structure and of being independent of the position chosen. However, it has been shown that the damping is far more sensitive to damage than the resonant frequency is. This is the reason to choose the damping measurements to evaluate the damage.

Two phases of the experimental work have been under taken. In the first phase of the work, the damage was simulated by milling-machine cuts. Three types of materials were considered in this phase of the work. They are SMC R50, Kevlar/epoxy, and hybrid composites. For the more realistic cases, the damage from three-point bending tests and artificial delaminations were considered in the second phase of the work. Two types of artificial delaminations were created. The first type of artificial delamination is represented by the insertion of 0.076 mm (0.003 in) thick mylar in two interfaces of $[90_5/0_4/90_5]$ glass/epoxy composite. The second type of artificial delamination is represented by the unglued portion in the middle plane of the 16-ply unidirectional glass/epoxy composite specimens. The three-point bending tests were performed by a Tinius Olsen testing machine on $[90_2/0_{10}/90_2]$ glass/epoxy specimens.

In both phases of the experimental work, the correlation between damage and damping was investigated to assess the ability of damping measurements to detect the damage.

In general, the severity of the damage simulated by the milling-machine cuts correlates well with increased damping for the first three modes of vibration. It has been shown that the sensitivity of damping to local damage for each mode of vibration depends on the positions of the damage. The lower mode is the most sensitive nearing the root and the higher mode is the most sensitive nearing the end of the specimen. With the understanding of the behaviors of damping to the presence of local damage, a proper way of damping measurements can be employed to detect the local damage. However, this technique has certain limitations. It is difficult to detect the damage below 5% of reduction in total thickness of the specimen. To detect the small damage, an ability for measurements of higher modes of vibration may be necessary.

The sensitivities of materials to the presence of local damage were compared. The SMC R50 is the most sensitive while Kevlar/epoxy is the least sensitive to the presence of the local damage. The sensitivity of hybrid composite G4 lies in the between.

In the second phase of the experimental work, damage from the more realistic cases were considered. There are no significant changes in the damping of the specimens having inserts at two interfaces of $[90_5/0_4/90_5]$ glass/epoxy

composite. This lack of expected damping enhancement is attributed to three factors: (1) The inserts being bonded with the material, (2) Material damping variation between the specimens being more than the damping change due to inserts, (3) The variation in damping due to clamping at the mounting base being more than the damping change caused by the mylar inserts.

The first factor can be improved by the artificial delamination represented by the unglued portion in the middle plane of the 16-ply unidirectional glass/epoxy specimens. The severity of the damage correlating well with increased damping has been observed. Thus, this type of damage can be detected by the damping measurements.

Measurements of damping from $[90_2/0_{10}/90_2]$ glass/epoxy specimens damaged by three-point bending tests have shown that no significant changes can be expected. This may be attributed to the fact that the damping changes due to the damage of matrix-crack type are masked in small amplitude of vibration by the non-homogeneity and by the losses occurring at the mounting base of the specimens.

Considerable efforts have been made to investigate the ability of damping measurements to detect damage. Once the damage is detected, it is desired to know the location and severity of the damage. The percent damping differences of the first three modes versus positions of damage for various severities of the damage have been plotted for this purpose. A graphic method was described to roughly locate and quantify

the damage from the measured damping values. The results of the method gave correct ranges in evaluations of the location and severity of the damage. The correctness of the method has been confirmed for the milling-machine-cut damage in materials of SMC R50, Kevlar/epoxy, and hybrid composite specimens. The ranges evaluated can be narrowed by offering more data points.

The equivalent percent reduction of total thickness can be used to measure the damage size in more realistic cases, for example, the damage from three-point bending tests. Thus, the method can be applied to locate and quantify the damage which results from other causes than the milling-machine cuts.

6.2. Conclusions

The impulse technique appears to be reliable for measuring internal material damping of composite materials. The use of the damping measurements for nondestructively assessing the integrity of fiber reinforced composite materials has been quite successful for the case of damage represented by milling-machine cuts. The technique used is quite capable to detect both severity and location of this type of damage. On the other hand, however, for damages introduced by artificial delaminations and three-point bending tests, the changes in damping are insignificant. Results may be improved if material damping variations

between specimens can be eliminated or measurements are performed on the same specimen.

It has been pointed out that damage less than 5% of reduction in total thickness of the specimen is difficult to detect. Thus, damping is not sensitive to microdamage (i.e., the damage in the order of the fiber diameter or less) within the frequency range measured (up to 1200 Hz). It is generally believed that to detect microdamage, the wave length should be in the same order or less than the microdamage. Consequently, it is necessary to be able to measure damping in higher modes of vibration. This requires more ability of identifying the response signal noise, filtering it out and also conditioning the signal.

The equivalent percent reduction of total thickness can be employed to evaluate approximately the severity of damage, although the technique is not sensitive to microdamage. The technique can be applied as a preliminary step to assess qualitatively the integrity of structures, and then other nondestructive testing techniques can be used to achieve the final evaluations.

APPENDIX A
DERIVATION OF EQS. (2.15) FOR THE CASES OF VISCOUS DAMPING AND COMPLEX STIFFNESS REPRESENTATION OF DAMPING

I. Viscous Damping

A. Derivation of $\delta = 2\pi\xi$

The differential equation of motion for free vibrations of a single degree of freedom viscously damped system has the form

$$m\ddot{x} + c\dot{x} + kx = 0 \tag{A.1}$$

where m is the mass of the system, c is the viscous damping coefficient, and k is the spring stiffness.

The solution of Eq. (A.1) is presented in detail on p. 26 of Thomson [44]. This solution of oscillatory motion is

$$x = e^{-(c/2m)t}(c_1 \cos\omega_d t + c_2 \sin\omega_d t) \tag{A.2}$$

where ω_d is the natural frequency of the damped motion, given by

$$\omega_d = \sqrt{(k/m) - (c^2/4m^2)} \tag{A.3}$$

and where c_1 and c_2 are arbitrary constants depending upon the initial conditions of the motion.

The critical damping coefficient, C_c, is the minimum value of c for which the free vibration motion is non-oscillatory. In the system of Eq. (A.1), the critical damping coefficient has the value of

$$C_c = 2\sqrt{km} \tag{A.4}$$

Define a damping ratio as

$$\xi = \frac{c}{C_c} \tag{A.5}$$

Then,

$$\frac{c}{2m} = \frac{C_c}{2m}\xi = \xi\omega_n$$

where ω_n is the natural frequency of the undamped motion, given by

$$\omega_n = \left(\frac{k}{m}\right)^{1/2} \tag{A.6}$$

Equation (A.3) becomes

$$\omega_d = \omega_n\sqrt{1 - \xi^2} \tag{A.7}$$

Thus, Eq. (A.2) can be rewritten as

$$x = e^{-\xi\omega_n t}(c_1\cos\sqrt{1 - \xi^2}\omega_n t + c_2\sin\sqrt{1 - \xi^2}\omega_n t) \tag{A.8}$$

The ratio of the displacements x(t) and x (t + τ) at times separated by one period $\tau = 2\pi/\omega_d$ of the oscillatory motion is

$$x(t)/x(t + \tau) = e^{-\xi\omega_n t}/e^{-\xi\omega_n(t + 2\pi/\omega_d)}$$

$$= e^{2\pi\xi/\sqrt{1 - \xi^2}} \tag{A.9}$$

The logarithmic decrement δ is then given by

$$\delta = \ln[x(t)/x(t + \tau)] = 2\pi\xi/\sqrt{1 - \xi^2} \tag{A.10}$$

For small damping, $\xi << 1$, Eq (A.10) can be approximated by

$$\delta = 2\pi\xi \tag{A.11}$$

B. Derivation of $\delta = \pi\eta$

The dissipated energy during one cycle of a harmonic motion was given in Eq. (2.2) by

$$D = \pi c\omega X^2 \tag{A.12}$$

where ω is the steady-state forced frequency and X is the amplitude of the motion.

Let U represent the peak potential or strain energy. Then,

$$U = \frac{1}{2}kX^2 \tag{A.13}$$

For small damping and excitation at resonant frequency, U is approximated by

$$U = \frac{1}{2}m\omega_n^2 X^2 \tag{A.14}$$

By the definition of loss factor, η, one obtains

$$\eta = \frac{D}{2\pi U} = \frac{c\omega}{m\omega_n^2} \tag{A.15}$$

Peak response frequency is known as $\omega_r = \omega_n\sqrt{1 - 2\xi^2}$.
Assuming small damping ($\xi << 1$), $\omega_r = \omega_n$.
For resonant excitation, $\omega = \omega_n$, Eq. (A.15) can be written as

$$\eta = \frac{C_c}{m\omega_n}\xi \tag{A.16}$$

For small damping, $\xi = \frac{\delta}{2\pi}$. Thus,

$$\eta = \frac{2m\omega_n}{m\omega_n}\frac{\delta}{2\pi} \tag{A.17}$$

which gives

$$\delta = \pi\eta \tag{A.18}$$

for resonant excitation.

II. Complex Stiffness Representation

According to p. 75 of Thomson [44], the structural damping can be represented by the complex stiffness

$k(1 + i\gamma)$ and the equation of motion of the free vibration can be written as

$$m\ddot{x} + k(1 + i\gamma)x = 0 \tag{A.19}$$

where γ is the dimensionless structural damping coefficient and $i = \sqrt{-1}$. Here a complex stiffness serves to represent both components of the force proportional to displacement, x. One component, kx, is in phase with the amplitude. The other component, $ik\gamma x$, is in phase with the velocity (90° ahead of the displacement) by virtue of the complex symbol i introduced into Eq. (A.19). The component, $ik\gamma x$, is the damping force.

The first step in this derivation is to verify the relationship between γ and η. The rate of energy dissipation with time is

$$\frac{dD}{dt} = f\frac{dx}{dt} \tag{A.20}$$

where f is the damping force, given by

$$f = k\gamma X\cos\omega t \tag{A.21}$$

for simple harmonic motion, $x = X\sin\omega t$.

The energy dissipated over a complete cycle will be

$$D = \int_0^{\frac{2\pi}{\omega}} k\gamma X^2\omega\cos^2\omega t\, dt = k\gamma X^2 \int_0^{2\pi} \cos^2\omega t\, d(\omega t) \tag{A.22}$$

$$= \pi k\gamma X^2$$

The peak strain energy is

$$U = \frac{1}{2} kX^2 \tag{A.23}$$

Thus, the loss factor is

$$\eta = \frac{D}{2\pi U} = \frac{\pi k \gamma X^2}{2\pi 1/2 k X^2} = \gamma \tag{A.24}$$

Equation (A.19) can then be written in the following form

$$m\ddot{x} + k(1 + i\eta)x = 0 \tag{A.25}$$

To solve Eq. (A.25), let

$$x = Xe^{st} \tag{A.26}$$

The characteristic equation is

$$ms^2 + k(1 + i\eta) = 0 \tag{A.27}$$

Let $s = a + ib$; then

$$m(a^2 + i2ab - b^2) + k(1 + i\eta) = 0$$

which can be separated into the two equations:

$$\begin{aligned} 2abm + k\eta &= 0 \\ m(a^2 - b^2) + k &= 0 \end{aligned} \tag{A.28}$$

Equations (A.28) give

$$a^2 = \frac{k}{2m}(-1 + \sqrt{1 + \eta^2}) \tag{A.29}$$

$$b^2 = \frac{k}{2m}(1 + \sqrt{1 + \eta^2}) \tag{A.30}$$

In Eq. (A.29), the negative value of a is to be taken, since this value represents a decay of the disturbance. Thus,

$$s_{1,2} = -(k/2m)^{1/2}(-1 + \sqrt{1 + \eta^2})^{1/2}$$

$$\pm i(k/2m)^{1/2}(1 + \sqrt{1 + \eta^2})^{1/2}$$

The solution of Eq. (A.25) is then

$$x = e^{-(k/2m)^{1/2}(-1 + \sqrt{1 + \eta^2})^{1/2}t}$$

$$\cdot [Ae^{i(k/2m)^{1/2}(1 + \sqrt{1 + \eta^2})^{1/2}t}$$

$$+ Be^{-i(k/2m)^{1/2}(1 + \sqrt{1 + \eta^2})^{1/2}t}] \qquad (A.31)$$

where A and B are arbitrary constants depending upon the initial conditions of the motion.

Equation (A.31) gives the amplitude ratio as

$$x(t)/x(t + \tau) = e^{(k/2m)^{1/2}(-1 + \sqrt{1 + \eta^2})^{1/2}\tau}$$

The logarithmic decrement is then given by

$$\delta = \ln[x(t)/x(t + \tau)]$$

$$= (K/2m)^{1/2}(-1 + \sqrt{1 + \eta^2})^{1/2}\tau \qquad (A.32)$$

For small damping, $\eta << 1$, the following approximations were made.

$$(1 + \eta^2)^{1/2} = 1 + \frac{1}{2}\eta^2$$

and

$$\tau = \frac{2\pi}{\omega_d} = \frac{2\pi}{\omega_n} = \frac{2\pi}{(k/m)^{1/2}}$$

Then, Eq. (A.32) reduces to

$$\delta = \pi\eta \tag{A.33}$$

Comparing Eqs. (A.11) and (A.33), shows that

$$\eta = 2\xi$$

for small damping.

This completes the derivation.

APPENDIX B
TABULATED DATA--MEASURED DAMPING VALUES FOR SMC R50 SPECIMENS

Specimen R50-1

Length 13.8 cm
Cross Section 2.54 cm x 0.244 cm
x/ℓ 0.033

(Δh/h)x100 (%)	$\eta_1 \times 10^4$	$\eta_2 \times 10^4$	$\eta_3 \times 10^4$
0	123.86	118.4	109.89
5	125.58	119.35	110.49
25	135.66	125.32	113.31
45	161.02	134.3	117.65
60	219.69	144.65	121.21
70	244.46	149.38	123.07

(Δh/h)x100 (%)	$\omega_1(H_z)$	$\omega_2(H_z)$	$\omega_3(H_z)$
0	63.09	396.9	1137.5
5	62.29	392.2	1131.2
25	57.42	375	1103.1
45	48.44	350	1062.5
60	35.74	326.6	1031.2
70	24.02	314.1	1015.6

Specimen R50-2

Length 13.8 cm
Cross Section 2.54 cm x 0.244 cm
x/ℓ 0.15

$(\Delta h/h)\times 100$ (%)	$\eta_1 \times 10^4$	$\eta_2 \times 10^4$	$\eta_3 \times 10^4$
0	128.57	123.77	116.96
5	128.99	123.77	117.3
25	134.35	124.54	117.65
45	147.19	125.32	118.34
60	176.92	126.38	119.4
70	224.62	126.64	119.76

Specimen R50-3

Length 13.8 cm
Cross Section 2.54 cm x 0.234 cm
x/ℓ 0.3

$(\Delta h/h) \times 100$ (%)	$\eta_1 \times 10^4$	$\eta_2 \times 10^4$	$\eta_3 \times 10^4$
0	100.85	126.43	119.05
5	101.19	127.45	119.4
25	103.28	128	121.95
45	110.32	130.22	127.79
60	126.21	134.3	137.45
70	165.35	140.23	149.25

Specimen R50-4

Length 13.8 cm
Cross Section 2.54 cm x 0.244 cm
x/ℓ 0.48

$(\Delta h/h)x100$ (%)	$\eta_1 \times 10^4$	$\eta_2 \times 10^4$	$\eta_3 \times 10^4$
0	127.34	121.27	114.28
5	127.75	121.77	114.28
25	128.57	125.85	114.28
45	132.4	135.83	114.28
60	139.81	154.32	113.69
70	164.33	188.57	114.94

Specimen R50-5

Length 13.8 cm
Cross Section 2.54 cm x 0.236 cm
x/ℓ 0.7

$(\Delta h/h)\times 100$ (%)	$\eta_1 \times 10^4$	$\eta_2 \times 10^4$	$\eta_3 \times 10^4$
0	101.19	130.22	123.46
5	101.7	131.93	124.89
25	101.7	133.41	128.2
45	101.7	140.58	137.92
60	103.28	161.8	154.33
70	105.83	192.6	168.77

Specimen R50-6

Length 13.8 cm
Cross Section 2.54 cm x 0.241 cm
x/ℓ 0.82

$(\Delta h/h)\times 100$ (%)	$\eta_1 \times 10^4$	$\eta_2 \times 10^4$	$\eta_3 \times 10^4$
0	133.73	128	121.21
5	132.94	128	121.21
25	131.63	128	122.7
45	131.7	128.54	128.2
60	131.1	132.23	142.34
70	131.36	142.59	170.2

Specimen R50-7

Length 13.8 cm
Cross Section 2.54 cm x 0.249 cm
x/ℓ 0.91

$(\Delta h/h)x100$ (%)	$\eta_1 \times 10^4$	$\eta_2 \times 10^4$	$\eta_3 \times 10^4$
0	124.18	118.4	111.77
5	123.95	117.94	112.68
25	123.03	118.4	112.99
45	122.28	117.48	113.64
60	121.32	117.94	115.94
70	121.32	117.94	121.95

APPENDIX C
TABULATED DATA--MEASURED DAMPING VALUES FOR KEVLAR/EPOXY SPECIMENS

Specimen KE--1

Length 24.1 cm
Cross Section 2.54 cm x 0.312 cm
x/ℓ 0.033

$(\Delta h/h)x100$ (%)	$\eta_1 \times 10^4$	$\eta_2 \times 10^4$	$\eta_3 \times 10^4$
0	43.02	42.13	31.75
5	43.21	42.31	31.75
25	45.66	43.59	32.21
45	50.76	45.16	33.01
60	61.54	46.22	33.73
70	81.63	47.09	34.37

Specimen KE--2

Length 24.1 cm
Cross Section 2.54 cm x 0.307 cm
x/ℓ 0.15

$(\Delta h/h)\times 100$ (%)	$\eta_1 \times 10^4$	$\eta_2 \times 10^4$	$\eta_3 \times 10^4$
0	44.05	43.6	31.75
5	44.44	43.69	31.95
25	45.98	43.79	32.16
45	50	43.98	32.57
60	57.31	43.89	33.01
70	67.11	44.36	33.72

Specimen KE--3

Length 24.1 cm
Cross Section 2.54 cm x 0.301 cm
x/ℓ 0.3

$(\Delta h/h)x100$ (%)	η_1 $x10^4$	η_2 $x10^4$	η_3 $x10^4$
0	45.15	44.57	32.21
5	45.53	44.77	32.36
25	46.19	45.08	33.01
45	48.78	45.9	34.61
60	53.98	47.32	36.91
70	60.79	48.94	38.97

Specimen KE--4

Length 24.1 cm
Cross Section 2.54 cm x 0.315 cm
x/ℓ 0.48

$(\Delta h/h) \times 100$ (%)	$\eta_1 \times 10^4$	$\eta_2 \times 10^4$	$\eta_3 \times 10^4$
0	43.67	42.76	30.76
5	43.67	42.94	30.81
25	43.86	43.79	30.81
45	44.74	46.76	30.9
60	47.17	53.97	30.95
70	50.13	60.35	31.35

Specimen KE--5

Length 24.1 cm
Cross Section 2.54 cm x 0.319 cm
x/ℓ 0.7

$(\Delta h/h)x100$ (%)	$\eta_1 \times 10^4$	$\eta_2 \times 10^4$	$\eta_3 \times 10^4$
0	43.76	42.85	31.75
5	43.86	42.39	31.95
25	43.96	43.22	32.79
45	43.86	44.57	34.36
60	44.15	50.61	38.3
70	44.54	56.29	40.92

Specimen KE--6

Length 24.1 cm
Cross Section 2.54 cm x 0.276 cm
x/ℓ 0.91

$(\Delta h/h)x100$ (%)	$\eta_1 \times 10^4$	$\eta_2 \times 10^4$	$\eta_3 \times 10^4$
0	47.85	46.76	33.67
5	47.85	46.76	33.72
25	47.73	46.76	33.73
45	47.62	46.87	34.13
60	47.51	46.87	34.6
70	47.51	47.09	36.09

APPENDIX D
TABULATED DATA--MEASURED DAMPING VALUES FOR HYBRID COMPOSITE G4 SPECIMENS

Specimen G4--1

Length 24.1 cm
Cross Section 2.5 cm x 0.434 cm
x/ℓ 0.033

$(\Delta h/h) \times 100$ (%)	$\eta_1 \times 10^4$	$\eta_2 \times 10^4$	$\eta_3 \times 10^4$
0	29.369	28.323	40.177
5	29.455	28.404	40.258
25	31.299	29.452	41.171
45	35.843	31.298	42.576
60	44.944	33.448	43.789
70	57.472	34.727	44.472

Specimen G4--2

Length 24.1 cm
Cross Section 2.5 cm x 0.457 cm
x/ℓ 0.15

$(\Delta h/h)x100$ (%)	$\eta_1 \times 10^4$	$\eta_2 \times 10^4$	$\eta_3 \times 10^4$
0	26.991	26.602	38.553
5	27.064	27.02	38.623
25	28.129	26.984	38.897
45	30.817	26.984	39
60	36.563	27.057	39.414
70	46.62	27.241	40.503

Specimen G4--3

Length 24.1 cm
Cross Section 2.51 cm x 0.391 cm
x/ℓ 0.3

$(\Delta h/h) \times 100$ (%)	$\eta_1 \times 10^4$	$\eta_2 \times 10^4$	$\eta_3 \times 10^4$
0	35.843	32.896	46.545
5	35.843	32.896	46.654
25	36.43	33.169	47.43
45	38.168	33.901	49.795
60	41.68	35.606	53.106
70	48.78	36.841	56.587

Specimen G4--4

Length 24.1 cm
Cross Section 2.51 cm x 0.401 cm
x/ℓ 0.48

$(\Delta h/h)\times 100$ (%)	$\eta_1 \times 10^4$	$\eta_2 \times 10^4$	$\eta_3 \times 10^4$
0	35.026	32	45.279
5	35.026	32.051	45.279
25	35.336	33.336	45.279
45	35.972	35.785	45.279
60	37.454	40.421	43.382
70	39.841	46.222	45.631

Specimen G4--5

Length 24.1 cm
Cross Section 2.53 cm x 0.437 cm
x/ℓ 0.7

$(\Delta h/h) \times 100$ (%)	$\eta_1 \times 10^4$	$\eta_2 \times 10^4$	$\eta_3 \times 10^4$
0	30.441	29.698	41.82
5	30.441	29.408	41.908
25	30.441	29.981	43.643
45	30.488	31.347	46.983
60	30.675	34.547	52
70	31.008	39.462	56.727

Specimen G4--6

Length 24.1 cm
Cross Section 2.53 cm x 0.432 cm
x/ℓ 0.82

$(\Delta h/h)x100$ (%)	$\eta_1 \times 10^4$	$\eta_2 \times 10^4$	$\eta_3 \times 10^4$
0	34.84	31.59	43.79
5	34.84	31.7	44.03
25	34.72	31.75	44.57
45	34.54	32.05	46.55
60	34.78	33.01	51.87
70	34.54	34.79	61.26

Specimen G4--7

Length 24.1 cm
Cross Section 2.53 cm x 0.455 cm
x/ℓ 0.91

$(\Delta h/h)x100$ (%)	$\eta_1 \times 10^4$	$\eta_2 \times 10^4$	$\eta_3 \times 10^4$
0	30.212	29.057	40.585
5	30.121	28.607	40.503
25	30.075	29.016	40.798
45	29.94	29.016	40.918
60	29.895	28.731	41.908
70	29.762	28.856	44.026

REFERENCES

1. Tober, G., and Schnell, H. Detectability of flaws in Boron and Carbon composite parts. AGARD-CP-234, 1978, pp. 17-1 to 17-5.

2. Adams, R.D., Cawley, P., Pye, C.J., and Stone, B.J. A vibration technique for non-destructively assessing the integrity of structures. Journal of Mechanical Engineering Science, Vol. 20, No. 2, 1978, pp. 93 to 100.

3. O'Brien, T.K., and Reifsnider, K.L. Fatigue damage evaluation through stiffness measurements in Boron-Epoxy laminates. Journal of Composite Materials, Vol. 15, January 1981, pp. 55 to 70.

4. O'Brien, T.K. Stiffness change as a nondestructive damage measurement. Mechanics of Nondestructive Testing edited by W.W. Stinchcomb, Plenum Press, New York, 1980, pp. 101 to 121.

5. O'Brien, T.K., and Reifsnider, K.L. Fatigue damage: Stiffness/strength comparison for composite materials. Journal of Testing and Evaluation, JTEVA, Vol. 5, No. 5, September 1977, pp. 384 to 393.

6. Dunegan, H.L., Harris, D.O., and Tatro, C.A. Fracture analysis by use of acoustic emission. Engineering Fracture Mechanics, Vol. 1, 1968, pp. 105 to 122.

7. Sims, G.D., Dean, G.D., Read, B.E., and Western, B.C. Assessment of damage in GEP laminates by stress wave emission and dynamic mechanical measurements. Journal of Materials Science, Vol. 12, 1977, pp. 2329 to 2342.

8. Rotem, A., and Altus, E. Fracture modes and acoustic emission of composite materials. Journal of Testing and Evaluation, JTEVA, Vol. 7, No. 1, January 1979, pp. 33 to 40.

9. Martin, G.G. In-flight acoustic emission monitoring. Mechanics of Nondestructive Testing edited by W.W. Stinchcomb, Plenum Press, New York, 1980, pp. 343 to 365.

10. Pollock, A.A. Quantitative evaluation of acoustic emission from plastic zone growth. International Advances in Nondestructive Testing (formerly International Journal of Nondestructive Testing), edited by W.J. McGonnagle, Vol. 6, Gordon and Breach Science Publishers, Inc., New York, 1979, pp. 239 to 261.

11. Prakash, R. Non-destructive testing of composite. Composites, Vol. 11, No. 4, October 1980, pp. 217 to 224.

12. Meron, M., Bar-Cohen, Y., and Ishai, O. Nondestructive evaluation of strength degradation in glass-reinforced plastics as a result of environmental effects. Journal of Testing and Evaluation, JTEVA, Vol. 5, No. 5, September 1977, pp. 394 to 396.

13. Williams, J.H., Jr., and Lampert, N.R. Untrasonic non-destructive evaluation of impact-damaged graphite fiber composite. NASA Contractor Report 3293, 1980.

14. Joshi, N.R., and Green, R.E. Ultrasonic detection of fatigue damage. Engineering Fracture Mechanics, Vol. 4, 1972, pp. 577 to 583.

15. Newhouse, V.L., and Furgason, E.S. Ultrasonic correlation techniques. Research Techniques in Nondestructive Testing--Volume III edited by R.S. Sharpe, Academic Press, New York, 1977, pp. 101 to 134.

16. Kaitatzidis, M. Inspection of carbon fibre parts after fabrication and during service. AGARD-CP-234, 1978, pp. 16-1 to 16-16.

17. Fitting, D.W., and Adler, L. Ultrasonic Spectral Analysis for Nondestructive Evaluation. Plenum Press, New York, 1981.

18. Pipes, R.B., editor. Nondestructive Evaluation and Flaw Criticality for Composite Materials, ASTM STP 696, American Society for Testing and Materials, Philadelphia, 1979, p. 96.

19. Chang, F.H., Gordon, D.E., and Gardner, A.H. A study of fatigue damage in composites by nondestructive testing techniques. ASTM STP 636, 1977, pp. 57 to 72.

20. Romano, T., Raymond, L., and Davis, L. Ultrasonic and X-ray radiographic inspection and characterization of defects in Gr/Al composites. Mechanics of Nondestructive Testing edited by W.W. Stinchcomb, Plenum Press, New York, 1980, pp. 293 to 307.

21. Halmshaw, R. Information theory applied to industrial radiography. Research Techniques in Nondestructive Testing--Volume II edited by R.S. Sharpe, Academic Press, New York, 1977, pp. 31 to 64.

22. Stone, D.E.W. Non-destructive inspection of composite materials for aircraft structural applications. AGARD-CP-234, 1978, pp. 14-1 to 14-18.

23. Bishop, R.E.D., and Johnson, D.C. The Mechanics of Vibration. Cambridge University Press, New York, 1979,

24. Springer, W.T. The vibrational characteristics of uniform bars containing a symmetric discontinuity in stiffness applied to structural integrity monitoring. Ph.D. Dissertation, The University of Texas at Arlington, 1982.

25. Cawley, P., and Adams, R.D. The location of defects in structures from measurements of natural frequencies. Journal of Strain Analysis, Vol. 14, No. 2, 1979, pp. 49 to 57.

26. Cawley, P., and Adams, R.D. A vibration technique for non-destructive testing of fibre composite structures. Journal of Composite Materials, Vol. 13, April 1979, pp. 161 to 175.

27. Lifshitz, J.M., and Rotem, A. Determination of reinforcement unbonding of composites by a vibration technique. Journal of Composite Materials, Vol. 3, July 1969, pp. 412 to 423.

28. Schrager, M. Fatigue as monitored by the torsion pendulum. Journal of Polymer Science A-2, Vol. 8, 1970, pp. 1999 to 2014.

29. Adams, R.D., Flitcroft, J.E., Hancox, N.L., and Reynolds, W.N. Effects of shear damage on the torsional behaviour of carbon fibre reinforced plastics. Journal of Composite Materials, Vol. 7, January 1973, pp. 68 to 75.

30. Gibson, R.F., and Plunkett, R. Dynamic mechanical behavior of fiber-reinforced composites: Measurement and analysis. Journal of Composite Materials, Vol. 10, October 1976, pp. 325 to 341.

31. Schultz, A.B., and Warwick, D.N. Vibration response: A non-destructive test for fatigue crack damage in filament-reinforced composites. Journal of Composite Materials, Vol. 5, July 1971, pp. 394 to 404.

32. Dibenedetto, A.T., Gauchel, J.V., Thomas, R.L., and Barlow, J.W. Nondestructive determination of fatigue crack damage in composites using vibration tests. Journal of Materials, Vol. 7, No. 2, June 1972, pp. 211 to 215.

33. Adams, R.D., Walton, D., Flitcroft, J.E., and Short, D. Vibration testing as a nondestructive test tool for composite materials. ASTM STP 580, 1975, pp. 159 to 175.

34. Steidel, R.F., Jr. An Introduction to Mechanical Vibrations. Second ed., chapter 6, John Wiley & Sons, Inc., New York, 1979.

35. Crandell, S.H. The role of damping in vibration theory. Journal of Sound and Vibration, Vol. 11, No. 1, January 1970, pp. 3 to 18.

36. Baker, W.E., Woolam, W.E., and Young, D. Air and internal damping of thin cantilever beams. Intl. J. Mech. Sci., Vol. 9, 1967, pp. 743 to 766.

37. Granick, N., and Stern, J.E. Material Damping of Aluminum by a Resonant Dwell Technique. NASA TN D-2893, National Aeronautics and Space Administration, 1965.

38. Schultz, A.G., and Tsai, S.W. Dynamic moduli and damping ratios in fiber-reinforced composites. Journal of Composite Materials, Vol. 2, No. 3, July 1968, pp. 368 to 379.

39. Halvorsen, W.G., and Brown, D.L. Impulse technique for structural frequency response testing. Sound and Vibration, November 1977, pp. 8 to 21.

40. Ottens, H.H. Mathematical formulation of damping for structural response analysis. AGARD-CP-277, 1979, pp. 1-1 to 1-10.

41. Kimball, A.L., and Lovell, D.E. Internal friction in solids. Physical Review Series 2, Vol. 30, 1927, pp. 948 to 959.

42. Lazan, B.J. Energy dissipation mechanisms in structures with particular reference to material damping. Structural Damping edited by J.E. Ruzicka, ASME, New York, 1959, p. 17.

43. Lazan, B.J. Damping studies in materials science and materials engineering. Internal Friction, Damping and Cyclic Plasticity, ASTM STP-378, American Society for Testing and Materials, Philadelphia, 1965, pp. 1 to 20.

44. Thomson, W.T. Theory of Vibration with Applications. Second ed., pp. 76 to 77, Prentice-Hall, Inc., New Jersey, 1981.

45. Stahle, C.V., and Forlifer, W.R. Ground vibration testing of complex structures. Proceedings of the 1958 Flight Flutter Testing Symposium, reprinted in NASA SP-385, 1975, pp. 83 to 90.

46. Lang, G.F. Understanding vibration measurements. Sound and Vibration, Vol. 10, No. 3, March 1976, pp. 26 to 37.

47. Bert, C.W. Material damping: An introductory review of mathematic models, measures and experimental techniques. Journal of Sound and Vibration, Vol. 29, No. 2, 1973, pp. 129 to 153.

48. Plunkett, R. Measurement of damping. Structural Damping edited by J.E. Ruzicka, ASME, New York, 1959, pp. 117 to 131.

49. Kume, Y., Hashimoto, F., and Maeda, S. Material damping of cantilever beams. Journal of Sound and Vibration, Vol. 80, No. 1, 1982, pp. 1 to 10.

50. Gibson, R.F., and Plunkett, R. A forced-vibration technique for measurement of material damping. Experimental Mechanics, Vol. 11, No. 8, August 1977, pp. 297 to 302.

51. Gibson, R.F., Yau, A., and Riegner, D.A. An improved forced vibration technique for measurement of material damping. Experimental Techniques, Vol. 6, No. 2, April 1982, pp. 10 to 14.

52. Ramsey, K.A. Effective measurements for structural dynamics testing. Part I, Sound and Vibration, Vol. 9, No. 11, November 1975, pp. 24 to 35.

53. Ramsey, K.A. Effective measurements for structural dynamics testing. Part II, Sound and Vibration, Vol. 10, No. 4, April 1976, pp. 18 to 31.

54. Drake, M.L., and Henderson, J.P. An investigation of the response of a damped structure using digital techniques. Shock and Vibration Bulletin, Vol. 45, Part 5, 1975, pp. 83 to 97.

55. Gordon, R.W., and Wolfe, H.F. Modal investigation of lightweight aircraft structures using digital techniques. Shock and Vibration Bulletin, Vol. 47, Part 3, 1977, pp. 61 to 77.

56. Henderson, J.P., and Drake, M.L. Vibration control using additive damping and FFT analysis. Society of Automotive Engineering, Inc., (SAE), Technical Paper Series, SAE-790220, 1979, pp. 1 to 14.

57. Bendat, J.S., and Piersol, A.G. Engineering Applications of Correlation and Spectral Analysis. Chapter 4, John Wiley & Sons, Inc., New York, 1980.

58. Bendat, J.S., and Piersol, A.G. Engineering Applications of Correlation and Spectral Analysis. Chaper 11, John Wiley & Sons, Inc., New York, 1980.

59. Mitchell, L.D. Signal processing with the Fast Fourier Transform (FFT) analyzer. SESA, Fall Meeting Proceedings, Salt Lake City, Utah, November 6-10, 1983, pp. 22 to 32.

60. Questions and answers--Structural analysis. Sound and Vibration, Vol. 17, No.2, February 1983, pp. 8 to 12.

61. Suarez, S.A., Gibson, R.F., and Deobald, L.R. Development of experimental techniques for measurement of damping in composite materials. SESA 1983 Fall Meeting Proceedings, Salt Lake City, Utah, November 6-10, 1983, pp. 55 to 60.

BIOGRAPHICAL SKETCH

Bai-Tang Lee was born in Taipei, Republic of China, on March 20, 1951. He attended Chung-Cheng Institute of Technology, Taoyuan, Taiwan, and received a Bachelor of Science in System Engineering in July of 1973. He was enrolled as a graduate student in Aeronautics and Astronautics at Stanford University in January, 1976. He received a Master of Science degree in Aeronautics and Astronautics in June, 1977. He married Yen-Jeng Chien on November 26, 1978. He has two daughters, Tzu-Ming and Tzu-Mei. After receiving a M.S. from Stanford University, he worked at C.C.I.T. as an instructor. In June, 1981, he enrolled in the Graduate School of the University of Florida for his Ph.D. degree. He will receive his Ph.D. in May, 1985. He will teach at C.C.I.T. when he returns to his country.

I certify that I have read this study and that in my opinion it conforms to acceptable standards of scholarly presentation and is fully adequate, in scope and quality, as a dissertation for the degree of Doctor of Philosophy.

Chang-Tsan Sun

Chang-Tsan Sun, Chairman
Professor of Engineering Sciences

I certify that I have read this study and that in my opinion it conforms to acceptable standards of scholarly presentation and is fully adequate, in scope and quality, as a dissertation for the degree of Doctor of Philosophy.

Mark H. Clarkson

Mark H. Clarkson
Professor of Engineering Sciences

I certify that I have read this study and that in my opinion it conforms to acceptable standards of scholarly presentation and is fully adequate, in scope and quality, as a dissertation for the degree of Doctor of Philosophy.

Ulrich H. Kurzweg

Ulrich H. Kurzweg
Professor of Engineering Sciences

I certify that I have read this study and that in my opinion it conforms to acceptable standards of scholarly presentation and is fully adequate, in scope and quality, as a dissertation for the degree of Doctor of Philosophy.

Lawrence E. Malvern

Lawrence E. Malvern
Professor of Engineering Sciences

I certify that I have read this study and that in my opinion it conforms to acceptable standards of scholarly presentation and is fully adequate, in scope and quality, as a dissertation for the degree of Doctor of Philosophy.

Arun Kumar Varma

Arun K. Varma
Professor of Mathematics

This dissertation was submitted to the Graduate Faculty of the College of Engineering and to the Graduate School, and was accepted as partial fulfillment of the requirements for the degree of Doctor of Philosophy.

May, 1985

Herbert A. Bruns

Dean, College of Engineering

Dean, Graduate School